Award Accounts

The Chemical Society of Japan Award for Young Chemists for 2007

Design of Porphyrin Nanoclusters toward Discovery of Novel Properties and Functions

Akihiko Tsuda

Department of Chemistry, Graduate School of Science, Kobe University, 1-1 Rokkodai-cho, Nada-ku, Kobe 657-8501

PRESTO, Japan Science and Technology Agency (JST), Sanbancho, Chiyoda-ku, Tokyo 102-0075

Received August 6, 2008; E-mail: tsuda@harbor.kobe-u.ac.jp

We have designed a variety of functional metalloporphyrin nanoclusters, connected via covalent or noncovalent linkages, since a discovery of fused bismetalloporphyrins $[Ar_3P]_2$(II) and $[Ar_3P]_2$(III) (Schemes 1–10 include symbols of the compounds), which have a strong π-electronic interaction over the bisporphyrin array. Among them, the following three topics are described in this review article. (1) Fused porphyrin nanoclusters: Directly fused oligoporphyrins, obtained through oxidative fused reactions of metalloporphyrins, show extremely strong π-electronic communications among the multiporphyrin components. (2) Self-assembled porphyrin nanoclusters: A zinc complex of meso–meso linked bisporphyrin $[PyP]_2$(I) bearing 4-pyridyl substituents, which allow Zn–N coordination interaction, forms a homochiral box-shaped cyclic tetramer $\{[PyP]_2(I)\}_4$. Its rotamers upon insertion of an oligoalkynylene bridge between the two porphyrin components $[PyP]_2(\equiv)_n$ ($n = 1$, 2, and 4) result in "conformational solvatochromism in nonpolar solvents" in $n = 2$ and "chiroptical sensing of asymmetric hydrocarbons" in $n = 4$, due to molecular recognition of solvents at the nanoscale cavity of box-shaped architecture. While a zinc porphyrin bearing a 3-pyridyl substituent (3-Py)P forms a cyclic tetramer with considerable structural distortion, its π-extended derivative (3-Py)P$(\equiv)_1$ bearing a trimethylsilylethynyl group shows "supramolecular thermochromism" with a vivid color change, due to a temperature-dependent self-assembling event. A supramolecular polymer of J-aggregated zinc porphyrin dendrimer DP can visualize chiroptically a macroscopic chirality of vortex flows, generated by mechanical rotary stirring of a fluid. (3) Inorganic–organic nanocomposites: A giant ring-shaped polyoxomolybdate cluster MC having a large cavity with a diameter of approximately 2.3 nm accommodates up to three molecules of aminophenyl-substituted metalloporphyrins TAP via hydrogen-bonding interactions, resulting in formation of discrete inorganic/organic inclusion complexes. Template-assisted cofacial assembly of MC by an oligomeric *p*-phenylenebutadiynylene rigid rod molecule bearing ammonium ion pendants PB_n allows formation of an inorganic/organic one-dimensional (1D) nano-object, having a polypseudorotaxane structure.

1. Introduction

π-Conjugated macrocycles, having chromophoric character, have potential applications such as optical, magnetic, and conductive materials, originating from the unique π-electronic networks on the cyclic structure.[1–7] In a variety of macrocycles, porphyrins with 22π-electrons, which obey Hückel's rule on aromaticity, have attracted great interest, since they play significant roles in nature such as in green leaves and red blood cells (RBC).[8,9] Light-harvesting antenna complexes with well-ordered metalloporphyrin derivatives allow efficient energy migration over many pigments within the antenna system toward a reaction center, while hemoglobin carrying four heme groups, consisting of an iron porphyrin derivative, allows oxygen transport from the lungs or gills to the rest of the body. These biological functions originate from the unique π-electronic structure and guest-hosting properties of the metalloporphyrin, together with well-ordered arrangements of the multi porphyrins. These characteristic features are dramatically variable upon attachment of certain substituents at the periphery of the porphyrin ring, modification of the macrocyclic ring, and insertion or exchange of the metal ion of the porphyrin center.[10–13] With these interesting features of the metalloporphyrins in mind, we have designed discrete metalloporphyrin clusters with an expectation of novel properties and functions, which can be only realized in an artificial system. Continuous challenges for making novel metalloporphyrin clusters with covalent and/or noncovalent linkages, under consideration of their potential specific functionalities, have allowed us to realize a variety of interesting phenomena, expected and unexpected.

2. History

We have initially succeeded in synthesis of fused bismetalloporphyrins $[Ar_3P]_2$(II) and $[Ar_3P]_2$(III) having strong π-electronic communication over the bisporphyrin array through

Published on the web January 14, 2009; doi:10.1246/bcsj.82.11

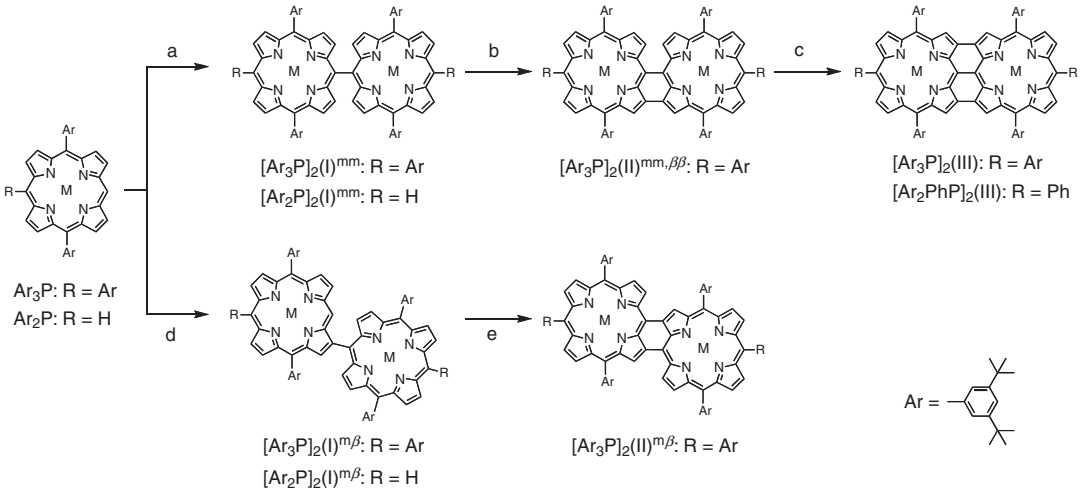

Scheme 1. Oxidative transformations of diaryl- and triaryl-substituted metalloporphyrins.[14–16,20,21]

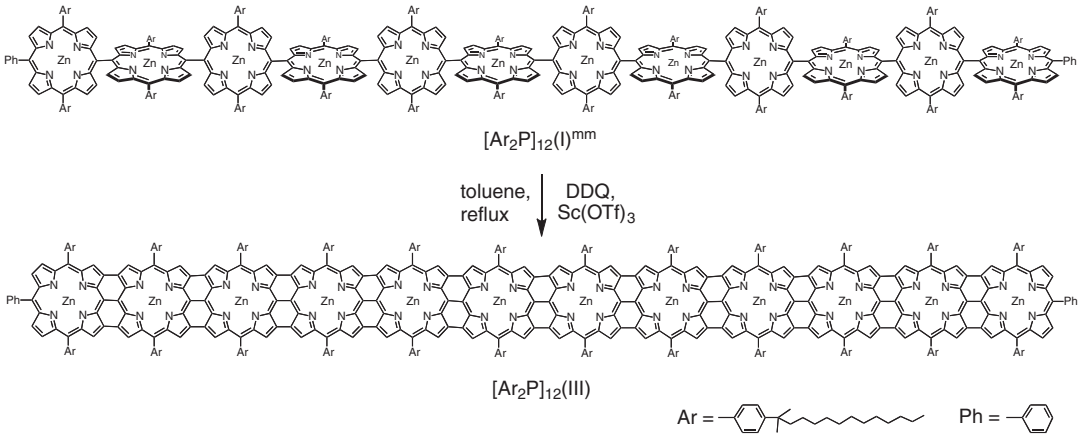

Scheme 2. Fully conjugated porphyrin tape formed upon oxidation of a meso–meso linked Zn^{II}–dodecaporphyrin with DDQ/$Sc(OTf)_3$.[17]

oxidative fused reactions of 5,10,15-triaryl-substituted metalloporphyrins Ar_3P with tris(4-bromophenyl)ammonium hexachloroantimonate (BAHA) (Scheme 1).[14–16] Consequently, their interesting π-electronic features prompted us to make longer arrays of the fused metalloporphyrin oligomers. A successful conversion of the meso–meso linked oligoporphyrins $[Ar_2P]_n(I)^{mm}$ ($n = 2$–12) into its completely fused form $[Ar_2P]_n(III)$ has been achieved in an oxidation reaction with 2,3-dichloro-5,6-dicyanobenzoquinone (DDQ) in the presence of $Sc(OTf)_3$ (Scheme 2).[17,18] Further, this finding has allowed us to synthesis meso-β fused oligoporphyrins $[Ar_2P]_n(II)^{m\beta}$ ($n = 2$–5), in which porphyrin components adopt an anti-arrangement, by oxidation of a nickel complex of Ar_2P with DDQ/$Sc(OTf)_3$ (Scheme 3).[19] Since the fused reactions proceed through oxidative couplings of metalloporphyrins,[20,21] where the porphyrin and oxidant initially occur as cation and anion radicals, respectively, the author hit upon the idea of stabilization of the anion radical of DDQ with Sc^{3+} via electrostatic interaction, based on previous research experience.[22,23] The author and Oshima have suggested previously a novel concept of "self-activated supramolecular reactions," where Diels–Alder reaction of a quinone derivative bearing an acyclic oligoether substituent with cyclopentadiene underwent 1.9×10^5 fold acceleration in the presence $Sc(OTf)_3$ (Scheme 4).[23] The oligoether chain binds Sc^{3+} in MeCN with the aid of a quinone carbonyl group to form a 1:1 noncovalent complex, which accelerates the electron-accepting character of quinone due to electron withdrawal toward Sc^{3+}. Since the fused oligoporphyrins obtained efficiently in this oxidation reaction are rich in π-electrons which communicate strongly over the multi porphyrin array, a variety of interesting applications using their derivatives have been developed in supramolecular chemistry and material sciences.[24,25]

In the course of X-ray crystallographic study of the bismetalloporphyrins, we noticed that $[Ar_3P]_2(I)^{mm}$ and $[Ar_2PhP]_2(III)$ in the crystal adopt a cyclotetrameric structure via intermolecular multiple CH–π interactions between alkyl substituents and the π-aromatic surface of the porphyrin ring (Figure 1c).[18] This finding motivated us, simply out of curiosity, to construct a possible dynamic large supramolecular assembly from the bismetalloporphyrin in solution. We have actually designed a box-shaped cyclic tetramer $\{[PyP]_2(I)\}_4$ from a zinc complex of meso–meso linked bisporphyrin $[PyP]_2(I)$ bearing 4-pyridyl substituents, which allow Zn–N coordination interaction in low polar solvents (Scheme 5).[26] Subsequent extension of the study by insertion of an

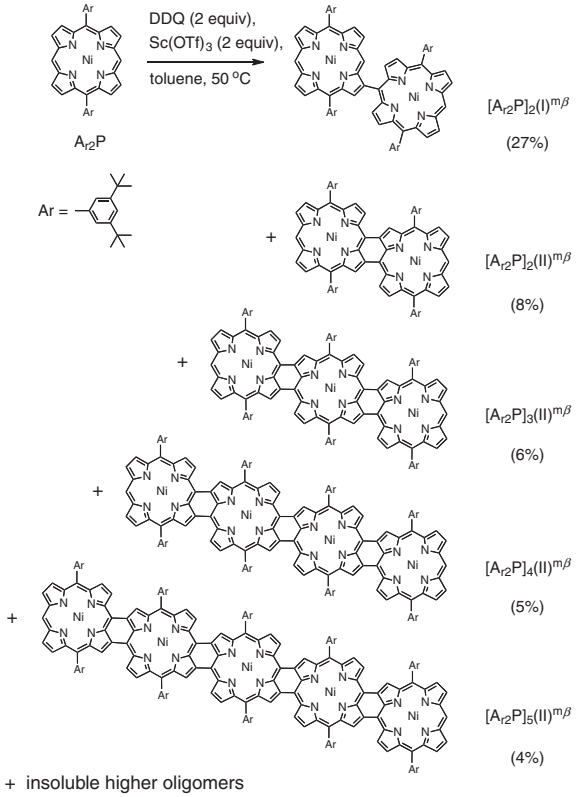

Scheme 3. Meso-β fused oligoporphyrins (2–5-mer) formed upon oxidation of a diaryl-substituted Ni^{II}–porphyrin with $DDQ/Sc(OTf)_3$.[19]

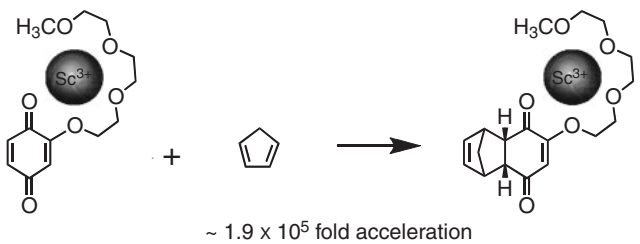

Scheme 4. Dramatic acceleration of Diels–Alder reaction of a quinone derivative, bearing an acyclic oligoether substituent, with cyclopentadiene in the presence of Sc^{3+}.[23]

oligoalkynylene bridge between the two porphyrin components $[PyP]_2(\equiv)_n$ ($n = 1$, 2, and 4) resulted in "conformational solvatochromism in nonpolar solvents" in $n = 2$ (Scheme 6 and Figure 8) and "chiroptical sensing of asymmetric hydrocarbons" in $n = 4$ (Scheme 6 and Figure 10), most likely due to molecular recognition of the solvent at the nanoscale cavity of the box-shaped architectures.[27–30] While in the course of a related study, we found that a zinc porphyrin bearing a 3-pyridyl substituent (3-Py)P forms a cyclic tetramer with considerable structural distortion, and its π-extended derivative of $(3\text{-Py})P(\equiv)_1$ bearing a trimethylsilylethynyl group showed a "supramolecular thermochromism" with a vivid color change by taking advantage of the temperature dependent self-assembling event (Figures 4 and 5).[31]

"Why does chiral symmetry breaking of the bisporphyrin box $\{[PyP]_2(\equiv)_4\}_4$ occur in asymmetric hydrocarbon solvents?"[30] Since the hydrocarbons do not possess functional groups appropriate for the formation of noncovalent bonds essential for stereochemical recognition, it is very much an important issue of study. In addition to the issue of molecular recognition, we also considered initially a possible certain chiral perturbation from the solvent outside of the cavity, and then hit upon an interesting idea of controlling the dynamic structure of the nanoscale assembly by chiral macroscopic forces such as a vortex. However, in the course of study, no chiroptical responses have been observed in bisporphyrin chiral boxes of $\{[PyP]_2(\equiv)_n\}_4$ under vortex flows generated upon rotary stirring of solutions. Since Brownian motions may be dominant over hydrodynamic interactions of molecular or nanoscale objects, it must be very difficult to cause hydrodynamic interactions of $\{[PyP_2](\equiv)_n\}_4$ with fluids. We then chose larger porphyrin supramolecular polymers with an expectation of hydrodynamic interactions with the fluids,[32] and found that their nanoscale fibrous assemblies such as J-aggregated zinc porphyrin dendrimer DP can chiroptically visualize the macroscopic chiral vortex flows, generated by mechanical rotary stirring of the solution in an optical cell (Scheme 7 and Figure 14).[34]

Concurrently with the studies on supramolecular porphyrin nanoclusters, we have also carried out construction of inorganic–organic nanocomposites from giant ring-shaped polyoxomolybdates (MC), developed by Müller and co-workers,[35] and metalloporphyrins or rod-shaped π-conjugated polymers (Schemes 8 and 9).[36,37] The author and co-workers have developed a variety of novel ideas, subjects, and findings from heterogeneous research fields upon integration of organic chemistry into different fields such as inorganic, polymer, and biological chemistries. Hence, here we chose inorganic MC for fabrication of novel inorganic–organic hybrid materials in expectation of interesting electronic and photochemical properties originating from its mixed-valent electronic structure. Here, MC was found to accommodate in its cavity 1–3 molecules of a metalloporphyrin with aminophenyl side groups TAP, forming inorganic/organic nanocomposite $MC\supset TAP_{1-3}$ (Scheme 8).[36] Based on this finding, we then successfully designed an inorganic–organic polypseudorotaxane, where a rod-shaped π-conjugated polymer (PB_n) bearing ammonium ion pendants threaded one-dimensionally the multiple MC rings in a cofacial manner by electrostatic interaction (Scheme 9).[37]

3. Fused Porphyrin Nanoclusters

Synthesis of π-conjugated porphyrin arrays with an extended π-electronic system has attracted considerable interest because of their remarkable electronic and photophysical properties such as high polarizability and high nonlinear optical (NLO) behavior.[38–42] Conjugated porphyrin arrays with an extremely low HOMO–LUMO gap are of current interest for their potential use in nanoscale molecular science.[39] In these studies, one of the central issues is to increase the electronic interaction between the porphyrin components and thereby to decrease HOMO–LUMO energy gap in order to achieve higher electric conductivity. Along this line, a variety of electronically conjugated multiporphyrin arrays, bridged by a π-conjugated unit such as oligoenes, oligoynes, and azo linkers, and edge-fused arrays by 1,4,5,8-tetraazaanthracene and benzene have

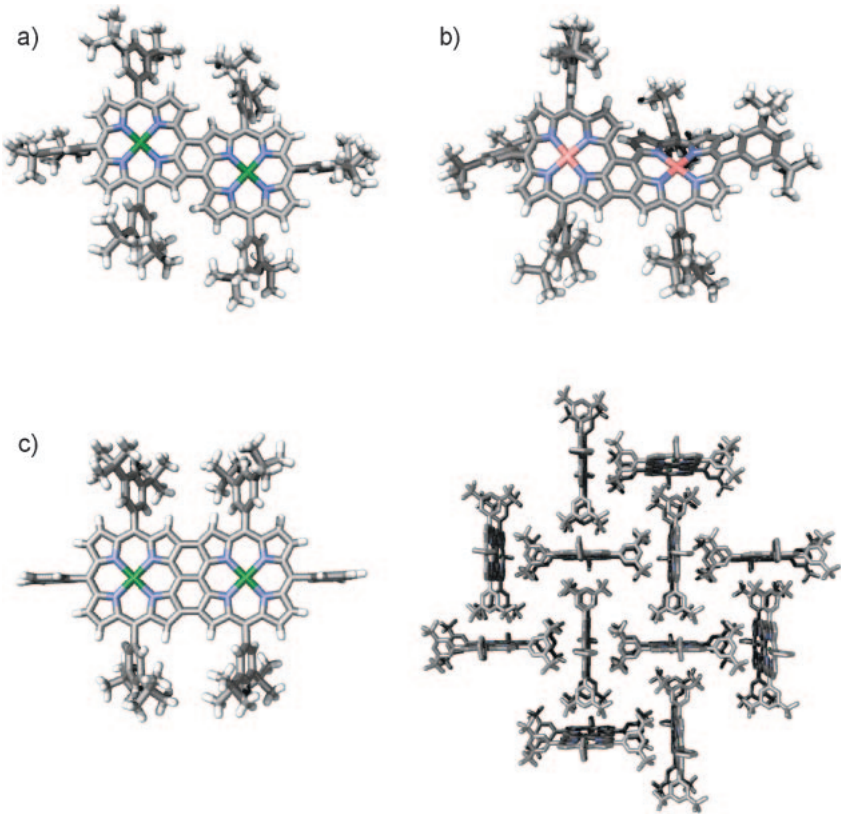

Figure 1. X-ray crystal structures of a) copper complex of meso-β fused bisporphyrin $[Ar_3P]_2(II)^{m\beta}$, b) nickel complex of meso–meso β–β fused bisporphyrin $[Ar_3P]_2(II)^{mm,\beta\beta}$, and c) copper complex of completely fused bisporphyrin $[Ar_2PhP]_2(III)$ and its 2D network structure, where hydrogen atoms are omitted for clarity.

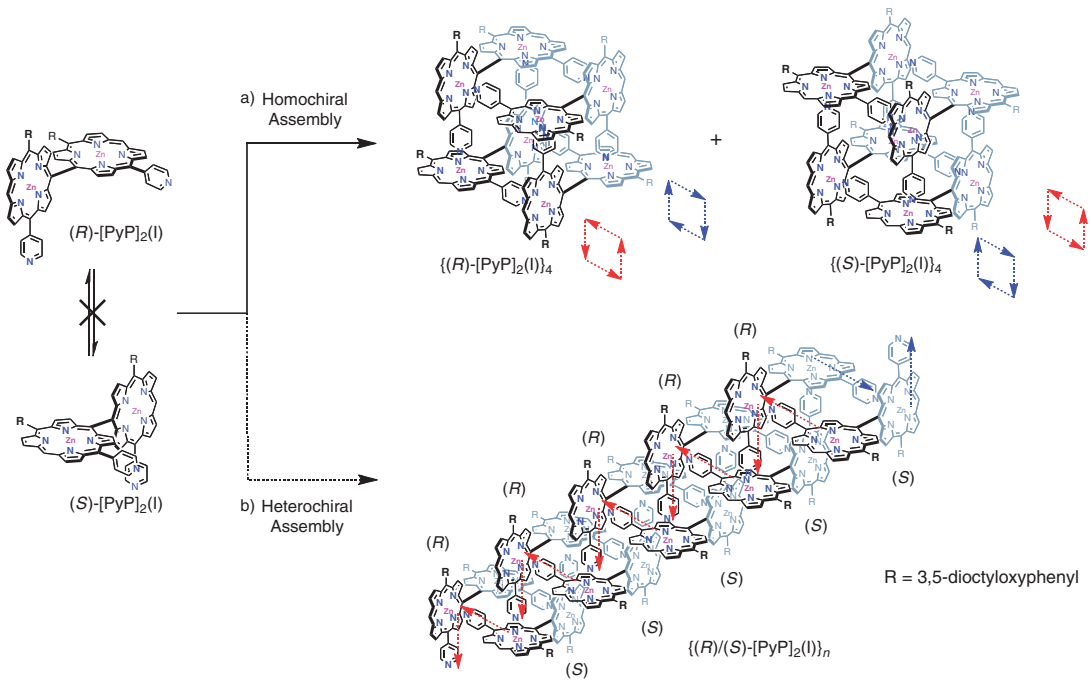

Scheme 5. Schematic representation of a racemic mixture of meso–meso linked Zn^{II}–bisporphyrin, bearing 4-pyridyl groups, and its self-assembling events. Red and blue arrows indicate the Py→Zn coordinating direction.[26]

been reported with their unique electronic properties.[38–42] With these backgrounds, we found that directly fused oligoporphyrins, obtained through oxidative fused reactions of metalloporphyrin, have extremely strong π-electronic communications over the multiporphyrin array (Schemes 1, 2, and 3).[14–19]

Oxidative coupling reactions of metalloporphyrins have

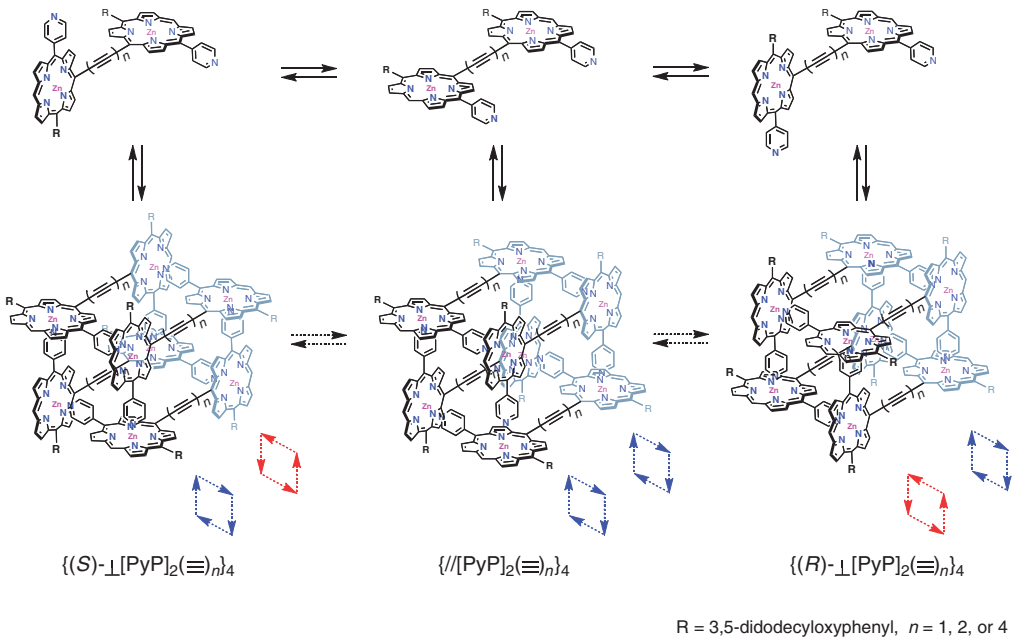

Scheme 6. Schematic representation of alkynylene-bridged Zn^{II}–bisporphyrin rotamers, bearing 4-pyridyl groups, and their self-assembling events. Red and blue arrows indicate the Py→Zn coordinating direction.[27–30]

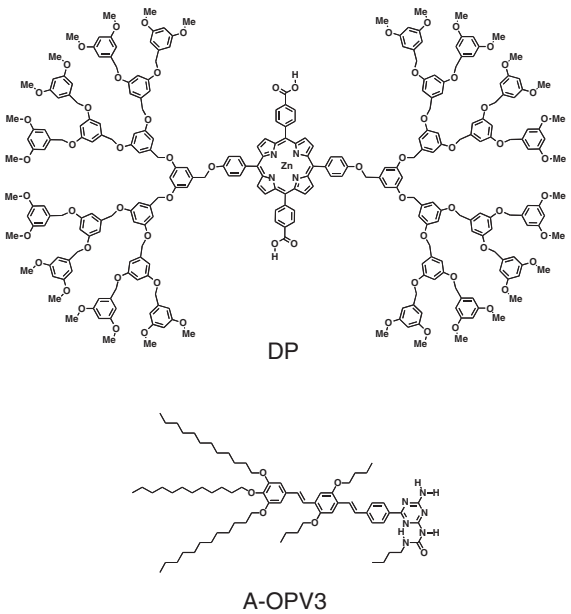

Scheme 7. Structural formulas of dendritic zinc porphyrin DP and oligo(*p*-phenylenevinylene) derivative A-OPV3.[33,34]

been actively studied by Osuka and co-workers since the discovery of a directly meso–meso linked zinc bisporphyrin $[Ar_2P]_2(I)^{mm}$ and the higher oligomers (Scheme 1, path a) formed upon one electron oxidation of a 5,15-diaryl-substituted Zn^{II}–porphyrin with Ag^{I} salt in $CHCl_3$.[20,43] They have also found that an electrochemical oxidation of Cu^{II}–, Ni^{II}–, and Pd^{II}–porphyrins allows formation of directly meso-β linked bismetalloporphyrins $[Ar_2P]_2(I)^{m\beta}$ (Scheme 1, path d).[21] The observed different coupling regioselectivity either giving $[Ar_2P]_2(I)^{mm}$ or $[Ar_2P]_2(I)^{m\beta}$ is most likely explained in terms of different HOMO orbital characters.[44] Zn^{II}–porphyrins favor A_{2u} HOMO in which there is large electron density at the meso carbon, whereas Cu^{II}–, Ni^{II}–, and Pd^{II}–porphyrins favor A_{1u} HOMO, which has nodal planes through the meso positions and has significant electron density at the β-positions.

After participation of the author in Osuka's group, we have achieved successful synthesis of fused bismetalloporphyrins through oxidation of metal complexes of Ar_3P, bearing a sterically uncongested meso position (Scheme 1).[14–16] Oxidation of Cu^{II}–, Ni^{II}–, and Pd^{II}–porphyrins gave rise to formation of meso-β fused bismetalloporphyrins $[Ar_3P]_2(II)^{m\beta}$ (Scheme 1, paths d and e), and the oxidation of meso–meso linked Cu^{II}–bisporphyrins $[Ar_3P]_2(I)^{mm}$ gave a completely fused bisporphyrin $[Ar_3P]_2(III)$ probably through meso–meso β–β fused bismetalloporphyrin $[Ar_3P]_2(II)^{mm,\beta\beta}$, as a possible intermediate (Scheme 1, paths b and c). Sugiura and co-workers have also reported the meso-β fused Ni^{II}–bisporphyrin $[Ar_2P]_2(II)^{m\beta}$ upon oligomerization reaction of a nickel complex of Ar_2P with $TeCl_4$.[45] Fortunately, we have obtained single crystals for the three types of fused bismetalloporphyrins, and demonstrated X-ray crystallography (Figure 1). In a copper complex of $[Ar_3P]_2(II)^{m\beta}$, the two porphyrin rings are forced to adopt a nearly coplanar conformation with a large ruffling and the mean plane deviation of 25 core atoms of 0.26 Å (Figure 1a). The C–C bonds of meso-β linkage are 1.46 Å, Cu–Cu distance is 8.66 Å, and mean Cu–N distance is 1.98 Å. However in a nickel complex of $[Ar_3P]_2(II)^{mm,\beta\beta}$, the two porphyrin rings take a nearly coplanar conformation, but with large ruffling toward the opposite directions (Figure 1b). The mean plane deviation is 0.34 Å, Ni–Ni distance is 8.20 Å, and mean Ni–N distance is 1.90 Å. As a result of the opposite ruffling, $[Ar_3P]_2(II)^{mm,\beta\beta}$ has a helical structure with nearly C_2 symmetry and the remaining two β-hydrogens adjacent to the meso–meso linkage are fixed to be about 3.20 Å apart. The helical structure of $[Ar_3P]_2(II)^{mm,\beta\beta}$ has been confirmed by

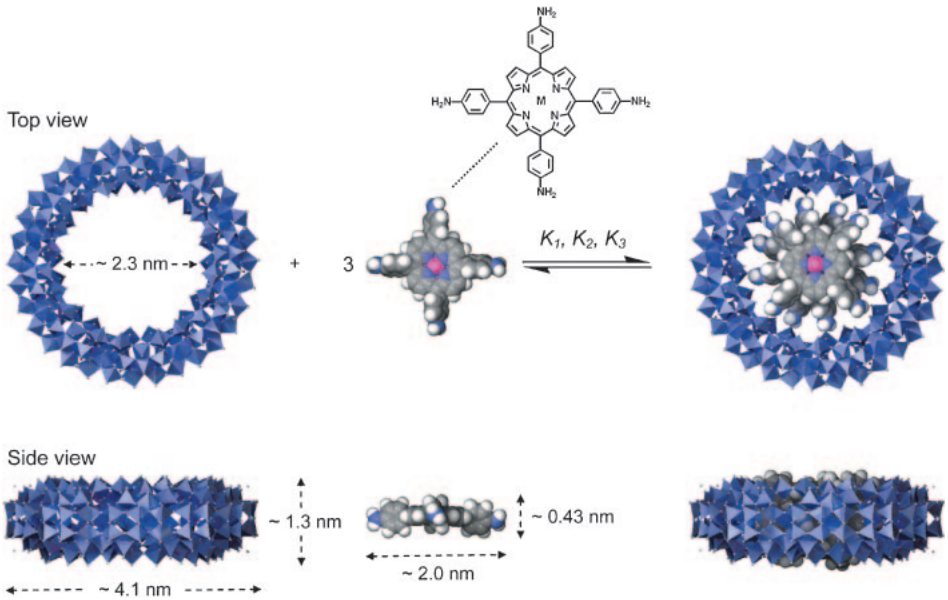

Scheme 8. Schematic representations of the complexation of a wheel-shaped polyoxomolybdate cluster (MC; blue polyhedra) with a zinc complex of 5,10,15,20-tetrakis(4-aminophenyl)porphyrin (TAP; space-filling model: pink Zn, blue N, gray C, white H).[36] Molecular models of MC and TAP are based on X-ray crystallography (see Ref. 35) and MM2 calculation, respectively.

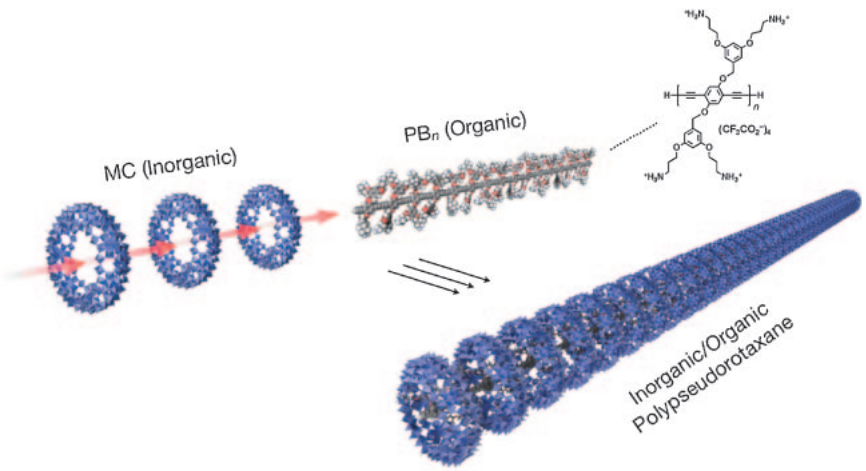

Scheme 9. Schematic illustration of inorganic/organic polypseudorotaxane derived from MC and PB_n.[37]

optical resolution of the two enantiomers using chiral HPLC. The activation barrier for the interconversion between the two enantiomers has been determined by monitoring the decrease of CD intensity in a toluene solution at 333–363 K. The racemization rate constants k_R that obey first-order kinetics have been determined at different temperatures, and the activation parameters ($\Delta G^{\ddagger} = 111\,\mathrm{kJ\,mol^{-1}}$, $\Delta H^{\ddagger} = 101\,\mathrm{kJ\,mol^{-1}}$, $\Delta S^{\ddagger} = -30.4\,\mathrm{J\,mol^{-1}\,K^{-1}}$, $\Delta E = 104\,\mathrm{kJ\,mol^{-1}}$) are obtained with similar values of those reported in a penta-helicene ($\Delta G^{\ddagger} = 101\,\mathrm{kJ\,mol^{-1}}$, $\Delta H^{\ddagger} = 95.8\,\mathrm{kJ\,mol^{-1}}$, $\Delta S^{\ddagger} = -17.2\,\mathrm{J\,mol^{-1}\,K^{-1}}$, $\Delta E = 98.3\,\mathrm{kJ\,mol^{-1}}$).[46] In sharp contrast to the largely ruffled structure of $[Ar_3P]_2(II)^{m\beta}$ and $[Ar_3P]_2(II)^{mm,\beta\beta}$, the two porphyrin rings in a copper complex of $[Ar_2PhP]_2(III)$ adopt a nearly coplanar structure with a very small mean plane deviation of 0.03 Å (Figure 1c, left). The C(β)–C(β) bonds are 1.41 Å long and C(meso)–C(meso) bond is 1.44 Å; Cu–Cu distance is 8.38 Å; mean Cu–N distance is 1.99 Å. In the crystal packing structure of $[Ar_2PhP]_2(III)$, it is interesting to note that $[Ar_2PhP]_2(III)$ shows orthogonal crystal packing with the 3,5-di-*tert*-butylphenyl groups pointing to the bisporphyrin surface to construct an infinite 2D-network by means of multiple CH/π interactions (Figure 1c, right).[18]

The oxidation potentials of the bismetalloporphyrins change systematically upon increment of the linkage between the porphyrin components.[16] The directly meso–meso linked Zn^{II}–bisporphyrin $[Ar_3P]_2(I)^{mm}$ underwent two reversible redox in oxidation at $E_{OX1} = 0.47$ and $E_{OX2} = 0.59$ V ($|\Delta E$ ($=E_{OX1} - E_{OX2})| = 0.12$ V) versus $Ag/AgClO_4$ due probably to one-electron redox in each porphyrin unit. The redox potentials in the first/second oxidation were also detected at 0.31/0.47 V ($|\Delta E| = 0.16$ V) for $[Ar_3P]_2(II)^{m\beta}$, and at 0.17/0.42 V ($|\Delta E| = 0.25$ V) for $[Ar_3P]_2(III)$, respectively. Within the same bismetalloporphyrin series, the first oxidation potentials decrease in the order of $[Ar_3P]_2(I)^{mm} > [Ar_3P]_2(II)^{m\beta} \geq$

$[Ar_3P]_2(II)^{mm,\beta\beta} > [Ar_3P]_2(III)$, suggesting an increase in energy of the HOMO orbital in this order. The $|\Delta E|$ values also increase in the reverse order of $[Ar_3P]_2(I)^{mm} < [Ar_3P]_2(II)^{m\beta} \leq [Ar_3P]_2(II)^{mm,\beta\beta} < [Ar_3P]_2(III)$, probably reflecting increased delocalization of the positive charge generated upon one-electron oxidation over the bismetalloporphyrin array.

All of the bisporphyrin set is available only for nickel porphyrins, and thus, their absorption spectra can be compared in Figure 2. In contrast to the sharp Soret band of the monomer Ar_3P (Figure 2a), the singly linked bisporphyrins $[Ar_3P]_2(I)^{mm}$ and $[Ar_2P]_2(I)^{m\beta}$ exhibit perturbed Soret bands but the spectral changes in the Q-bands are rather modest despite the direct connections (Figures 2b and 2c, respectively). The Soret band of $[Ar_3P]_2(I)^{mm}$ is split at 418 and 450 nm, and that of $[Ar_2P]_2(I)^{m\beta}$ is observed as a broad band with a peak at 412 nm with a shoulder at 425 nm, and the Q-bands are observed at 538 and 526 nm for $[Ar_3P]_2(I)^{mm}$ and $[Ar_2P]_2(I)^{m\beta}$, respectively. The spectral differences of $[Ar_3P]_2(I)^{mm}$ and $[Ar_2P]_2(I)^{m\beta}$ may be ascribed to their almost perpendicular conformations,[47] and can be qualitatively understood in terms of the exciton coupling between the transition dipole moments of the porphyrin, which depends on the oscillator strength and the relative geometry of the interacting transition dipole moments. A large electronic interaction between the two porphyrin components occurs in $[Ar_3P]_2(I)^{mm}$ and $[Ar_2P]_2(I)^{m\beta}$, but they are not conjugated. In contrast, the electronic π-systems in the fused bisporphyrins $[Ar_3P]_2(II)^{m\beta}$, $[Ar_3P]_2(II)^{mm,\beta\beta}$, and $[Ar_3P]_2(III)$ can be regarded as conjugated, by judging from their entirely perturbed absorption spectra (Figures 2d and 2e, respectively). Evidently, the forced coplanar geometries of the fused bisporphyrins allow the π-conjugation. The absorption spectra of the fused bisporphyrins $[Ar_3P]_2(II)^{m\beta}$ and $[Ar_3P]_2(II)^{mm,\beta\beta}$ are similar to each other, but the completely fused $[Ar_3P]_2(III)$ displays the most altered absorption spectrum with the largest splitting of the Soret-like band and extension of its Q-band into the near-infrared region (Figure 2f). Dramatic decrease of HOMO–LUMO energy gap due to strong π-electronic interaction in the completely fused form may result in such largely red-shifted absorption spectrum.

BAHA oxidation provided the fused bismetalloporphyrins accompanied by undesirable porphyrins halogenated at pyrrole β-positions. Chromatographic separation of these halogenated side products was an essential problem in the reactions, and thus, the BAHA oxidation was hardly applicable to synthesis of the higher fused oligoporphyrin arrays. We then found that $DDQ/Sc(OTf)_3$ oxidation of porphyrins in toluene under reflux allows fused reactions in good yield without observable peripheral halogenations.[17,48] This synthetic method was applicable to the higher meso–meso linked Zn^{II}–oligoporphyrins (up to 12-mer) to give the corresponding completely fused oligoporphyrins in 62–91% yield (Scheme 2). The completely fused zinc porphyrin arrays have planar tape-shaped structures, and display extremely red-shifted absorption bands, reflecting extensive π-conjugated electronic systems over the array (Figures 3a and 3b). Most notably, the lowest energy electronic absorption bands red-shifted dramatically and intensified upon increase of the number of the porphyrins, and extend into the IR region. The longest fused array, the 12-mer, exhibits a lower lying electronic excitation band with a peak around 3500 cm^{-1} and tail reaching ca. 1500 cm^{-1}. A plot of the absorption peak of the lowest energy band in wavelength units (λ_{max}) versus the number of porphyrins (N) revealed fairly linear behavior up to the dodecamer. At this stage, there is no detectable effective conjugation length (ECL).[49] The one-electron oxidation potentials also decrease steadily upon increase in the number of porphyrins (E_{ox}[V] vs. $AgClO_4/Ag = 0.21$ for 2-mer, –0.09 for 4-mer, –0.18 for 6-mer, and –0.24 for 8-mer).

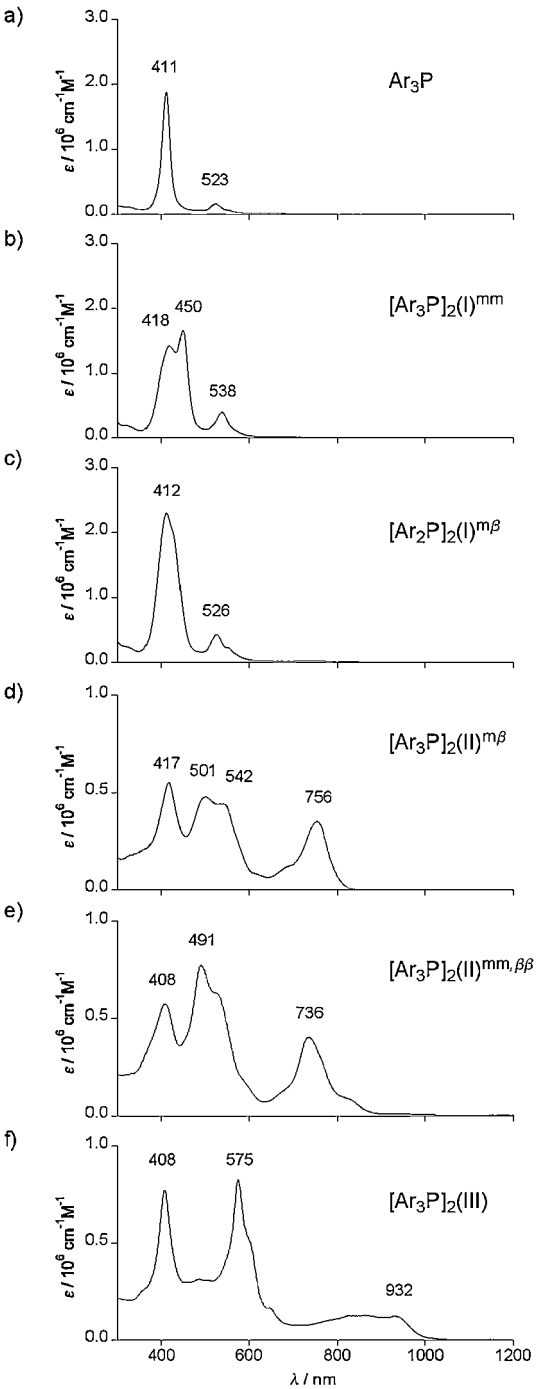

Figure 2. Absorption spectra of nickel complexes of a) Ar_3P, b) $[Ar_3P]_2(I)^{mm}$, c) $[Ar_2P]_2(I)^{m\beta}$, d) $[Ar_3P]_2(II)^{m\beta}$, e) $[Ar_3P]_2(II)^{mm,\beta\beta}$, and f) $[Ar_3P]_2(III)$ in $CHCl_3$.

We have also succeeded in synthesis of meso-β fused Ni^{II}-oligoporphyrins $[Ar_2P]_n(II)^{m\beta}$ ($n = 2$–5), in which porphyrin

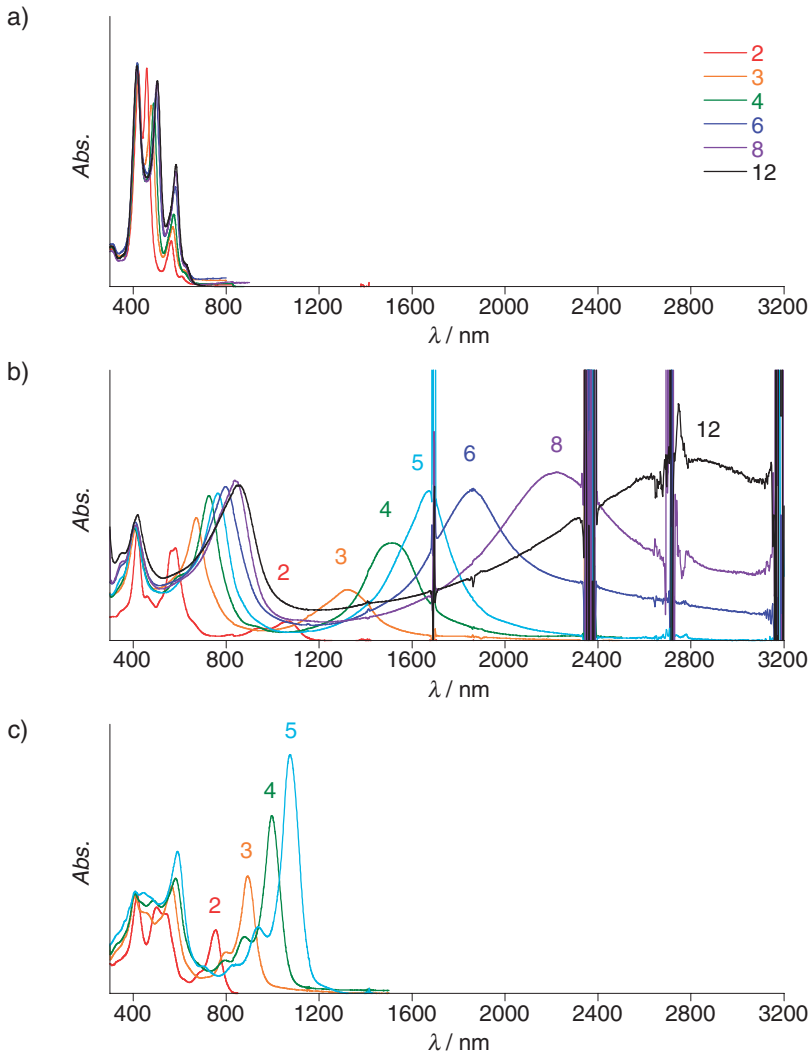

Figure 3. Absorption spectra of a) meso–meso linked Zn^{II}–oligoporphyrins $[Ar_2P]_n(I)^{mm}$ ($n = 2$–12), b) completely fused Zn^{II}–oligoporphyrins $[Ar_2P]_n(III)$ ($n = 2$–12), and c) meso-β fused Ni^{II}-oligoporphyrins $[Ar_2P]_n(II)^{m\beta}$ ($n = 2$–5) in $CHCl_3$.

components only adopt an anti-arrangement, by oxidation of a nickel complex of Ar_2P with DDQ/$Sc(OTf)_3$ in toluene at 50 °C (Scheme 3).[19] The one-electron oxidation potential of the meso-β fused bisporphyrin $[Ar_2P]_2(II)^{m\beta}$ is 0.56 V versus $AgClO_4/Ag$ in $CHCl_3$ solution, which is considerably lower than the values for a nickel complex of the directly meso-β linked bisporphyrin $[Ar_2P]_2(I)^{m\beta}$ (0.76 V) but higher than that for completely fused $[Ar_3P]_2(III)$ (0.46 V). Therefore, the HOMO energy level may be lifted upon expansion of the π-system of the porphyrin. This trend is enhanced upon increase of the number of the porphyrins (E_{ox}[V] vs. $AgClO_4/Ag$ = 0.44 for 3-mer, 0.38 for 4-mer, and 0.35 for 5-mer), where a plot of the one-electron oxidation potentials versus $1/N$ constitutes a good straight line. The intercept (0.21 V) of the plot may be assigned for the one-electron oxidation potential of the "infinite" meso-β fused oligoporphyrin array. The electronic absorption spectra of $[Ar_2P]_n(II)^{m\beta}$ ($n = 2$–5) exhibit roughly three regions as such in the meso–meso linked oligoporphyrins and completely fused oligoporphyrins (Figure 3c). The lowest energy band is progressively red-shifted and enhanced upon an increase of the number of the porphyrins. A plot of the absorption maxima (λ_{max}) of the lowest energy band versus the number of porphyrins (N) provided a non linear profile, but versus the reciprocal number of porphyrins in the array ($1/N$) gave a straight line, indicating the ECL effect.[49] Its intercept is around 1480 nm (6770 cm^{-1}) and may correspond to a limiting value of this array.

The extremely small HOMO–LUMO gaps, the exceedingly low oxidation potentials, and the long linear rigid molecular shapes of the higher fused oligoporphyrins encourage their potential use as conductive molecular wires. In addition, the unusual photophysical and electrochemical properties of these fused porphyrin arrays lend them to a number of potential avenues for further investigation, including the development of near-IR and IR sensors and dyes, and materials for nonlinear optics and spin-ordering.

4. Self-Assembled Porphyrin Nanoclusters

4.1 Thermochromism of a π-Extended Zinc Porphyrin Nanocluster. Porphyrins and metalloporphyrins can form a variety of well-defined nanoscale architectures via noncovalent interactions such as hydrogen bonding and coordination

bonding interactions.[11,13] These interactions occurring at the porphyrin center, with accompanying chromophoric interactions such as exciton coupling, upon self-assembly provide dramatic changes in electronic absorption spectra with certain color change. With this basic concept, we have found an interesting example of a "supramolecular multicolor thermometer" operating at ambient temperatures.[31] The system consists of a self-assembled zinc porphyrin complex (3-Py)P(≡)$_1$ bearing a 3-pyridyl group and an alkynyl group, whose association/dissociation dynamics in toluene leads to a stepwise absorption spectral change with vivid color change from green to yellow to red on heating from 0 to 50 to 100 °C, respectively (Figure 4). The observed color change includes a contribution of the exciton coupling among self-assembled (3-Py)P(≡)$_1$,[50] which turns on and off synchronously to the above coordination dynamics on assembly and dessembly. On the other hand, the alkynyl sidearm contributes to a shift of the absorption band of the complex, so that the absorption spectral change can be detected as a vivid switching between warm and cold colors by human eyes. CSI-MS of (3-Py)P(≡)$_1$,[51] together with ^{1}H NMR spectroscopy and X-ray crystallography of a reference complex of (3-Py)P, has indicated that (3-Py)P(≡)$_1$ preferentially adopts a cyclic tetramer with a considerable structural distortion (Figure 5).[52] The present system is a novel multicolor thermometer, which takes great advantage of the molecular design flexibility of metalloporphyrins.

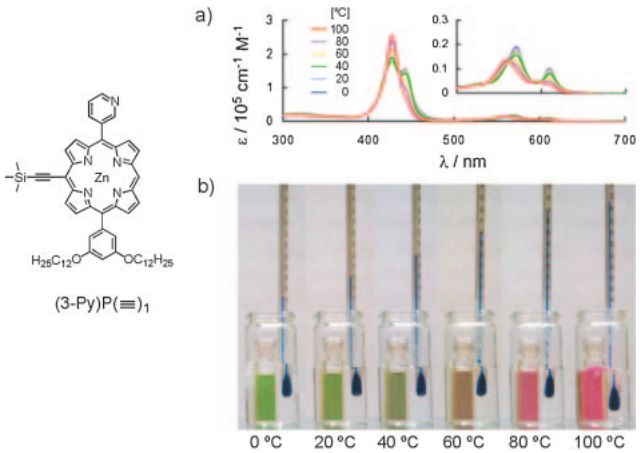

Figure 4. Variable-temperature a) absorption spectral profile and b) color profile of (3-Py)P(≡)$_1$ in toluene (9.8×10^{-5} M) at 0–100 °C (blue: 0 °C, red: 100 °C). Inset shows magnified spectra in the Q-band region.[31]

4.2 Conformational Solvatochromism with a Zinc Bisporphyrin Supramolecular Box. Zinc complex of 4-pyridine-appended porphyrins, such as 5-(4-pyridyl)-15-(3,5-di-*tert*-butylphenyl)porphyrinato zinc PyP, self-assembles to form a cyclic tetramer with a square geometry both in solution and in the solid-state (Figure 6).[53] We have successfully extended this event to the self-assembly of a directly meso–meso linked Zn^{II}–bisporphyrin [PyP]$_2$(I), to furnish a porphyrin nano box {[PyP]$_2$(I)}$_4$ with enhanced stability (Scheme 5).[26b] The cyclic tetramerization of [PyP]$_2$(I) was characterized by means of size-exclusion chromatography (SEC), ^{1}H NMR, electronic absorption, and fluorescence spectroscopy, together with cold spray ionization mass spectrometry (CSI-MS).[51] A THF solution of [PyP]$_2$(I) in CSI-MS actually provided the parent ion peak of {[PyP]$_2$(I)}$_4^+$ at 6258 (calcd for $C_{376}H_{400}N_{40}O_{16}Zn_8$ 6258) (Figure 7). Here, it must be noted

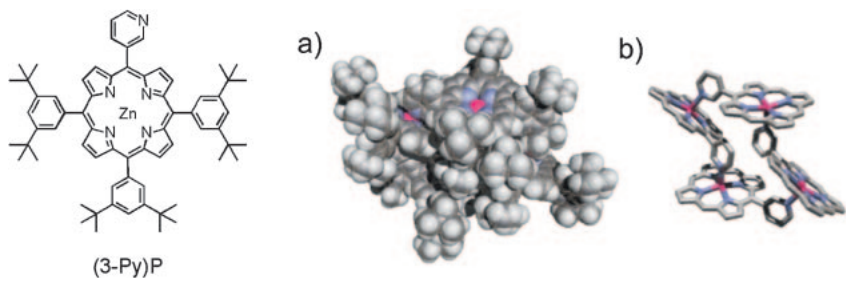

Figure 5. X-ray crystal structure of (3-Py)P. a) CPK representation. b) Stick representation, where 3,5-di-*tert*-butylphenyl groups and hydrogen atoms are omitted for clarity.

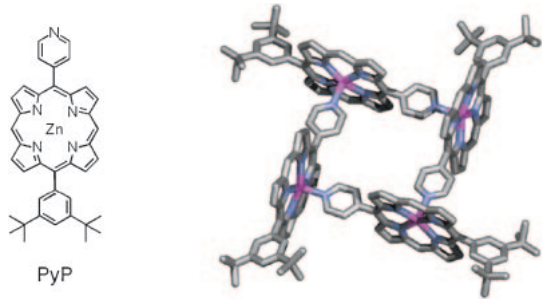

Figure 6. X-ray crystal structure of PyP. Hydrogen atoms are omitted for clarity.

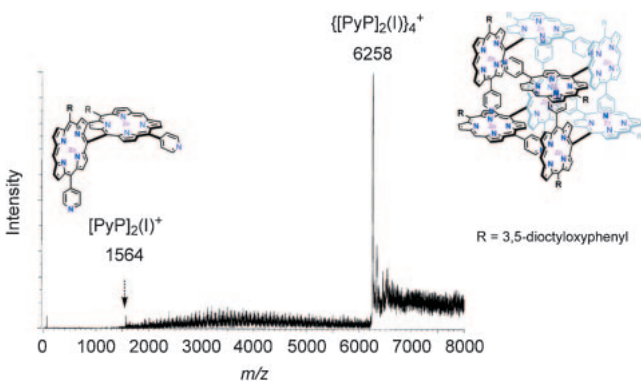

Figure 7. Cold spray ionization mass spectrometry (CSI-MS) of {[PyP]$_2$(I)}$_4$ in THF.

that directly meso–meso linked bisporphyrins have no rotational freedom of the porphyrin components around the meso–meso linkage due to steric hindrance of hydrogens attached at pyrrole-β positions, and thus, $[PyP]_2(I)$ is chiral, having R or S configurations (Scheme 5).[47] The racemic mixture of $[PyP]_2(I)$ thus has a capability to form a cyclic tetramer (path a) and/or a supramolecular ladder polymer (path b), composed of homochiral or heterochiral bisporphyrin components, respectively. However interestingly, $[PyP]_2(I)$ forms the former discrete assembly as a sole product. Large enthalpic gain of the ring-closed system may allow dominant formation of the cyclic tetramer. Later, Osuka and co-workers actually succeeded in separating enantiomers of $\{(R)\text{-}[PyP]_2(I)\}_4$ and $\{(S)\text{-}[PyP]_2(I)\}_4$ by means of chiral HPLC on SUMICHIRAL OA-3100 column using CH_2Cl_2/hexane (3:7) as an eluent.[26a]

As an extension of the study, we have designed alkynylene-bridged Zn^{II}–bispyridylporphyrin rotamers $[PyP]_2(\equiv)_n$ ($n = 1$, 2, and 4), having rotational freedom of the porphyrin components around the alkynylene axis (Scheme 6).[27–30] $[PyP]_2(\equiv)_n$ self-assemble to form box-shaped homochiral and achiral cyclic tetramers ($\{\perp[PyP]_2(\equiv)_n\}_4$ and $\{//[PyP]_2(\equiv)_n\}_4$), where $[PyP]_2(\equiv)_n$ is conformationally frozen to adopt perpendicular and planar conformations, respectively. When $n = 1$, the planar conformer is always selected because of a strong energetic gain by the extension of a π-electronic conjugation.[27] When $n = 2$, the mole fraction of the two conformers is highly dependent on the solvent.[28,29] Namely, $\{[PyP]_2(\equiv)_2\}_4$ with a variable extent of π-conjugation shows a unique solvatochromic response to nonpolar solvents with equally low dielectric constants (2.23–2.57) (Figure 8).[29] Most explicit is the case with CCl_4, where $\{//[PyP]_2(\equiv)_2\}_4$ was selected almost perfectly despite the fact that its dielectric constant is close to that of benzene with an opposite preference to $\{\perp[PyP]_2(\equiv)_2\}_4$. Further, it can spectroscopically discriminate the regioisomers of xylene, where "%-stereoisomeric excess" (%se) values, defined by $(\{//[PyP]_2(\equiv)_2\}_4 - \{\perp[PyP]_2(\equiv)_2\}_4)/(\{//[PyP]_2(\equiv)_2\}_4 + \{\perp[PyP]_2(\equiv)_2\}_4) \times 100$ are 39% and −78% in *o*- and *p*-xylene, respectively (Figure 9), while the color of free-base $[PyP]_2(\equiv)_2$, unassembled reference, was not solvent-dependent. These observed events take advantage of a confined chromophoric cavity,[54] given by the assembly of a π-conjugated rotamer with a variable extent of π-conjugation, and thus, can be referred to as "conformational" solvatochromism. In principle, solvatochromic shifts are caused by a change in the energy gap between the ground state and excited state having different polarities, since a change in the solvent polarity leads to differential stabilization of these electronic states.[55,56] However, $[PyP]_2(\equiv)_2$ shows explicit solvatochromic response to the nonpolar solvents due probably to particular electronic and/or steric effects of caged solvent molecules on their interaction with the cavity of hosting $\{[PyP]_2(\equiv)_2\}_4$.

4.3 Chiroptical Sensing of Asymmetric Hydrocarbons Using a Chiral Supramolecular Box. A variety of new concepts of chiral molecular reactions have been developed in supramolecular chemistry.[57] Certain achiral or dynamically racemic substances show a chiroptical response upon interaction with optically active species, where the chiral molecular recognition, being allowed by multipoint interactions, biases thermodynamic stability of resulting stereoisomers of the noncovalent complex. The dynamic structural conversion, induced upon chirality transfer with chemical or physical stimuli, is one of the most interesting subjects of supramolecular chiral chemistry.[58–60] In such events, porphyrins

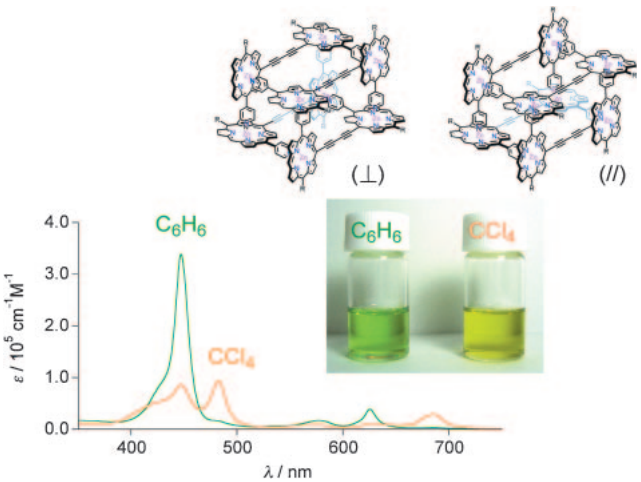

Figure 8. Absorption spectra of $\{[PyP]_2(\equiv)_2\}_4$ at 20 °C in benzene (green) and CCl_4 (yellow). Inset shows pictures of benzene (left) and CCl_4 (right) solutions of $\{[PyP]_2(\equiv)_2\}_4$.[29]

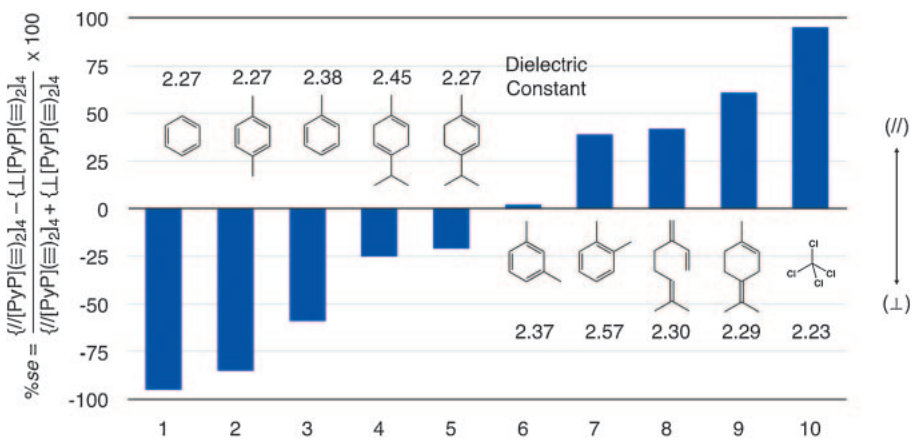

Figure 9. %-Stereoisomeric excess (%se) values of $\{[PyP]_2(\equiv)_2\}_4$ in nonpolar solvents at 20 °C ($[PyP]_2(\equiv)_2 = 5.9 \times 10^{-6}$ M).

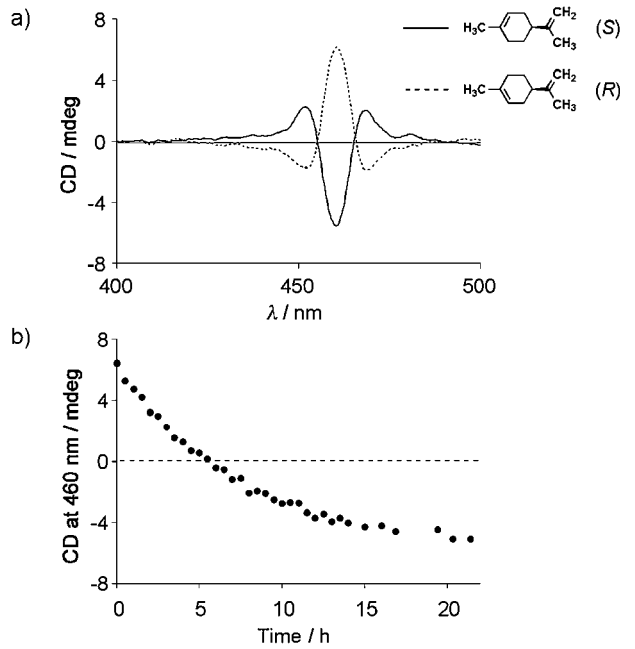

Figure 10. a) Circular dichroism (CD) spectroscopy of $\{\perp[PyP]_2(\equiv)_4\}_4$ ($[PyP]_2(\equiv)_4 = 1.6 \times 10^{-6}$ M) at 20 °C in (*R*)- and (*S*)-limonene (solid and broken curve, respectively). b) Plots of CD intensity at 460 nm after 100-fold dilution of an (*S*)-limonene solution of $[PyP]_2(\equiv)_4$ (0.03 mL, $\{[PyP]_2(\equiv)_4\}_4 = 1.6 \times 10^{-4}$ M) with 3.0 mL of (*R*)-limonene.[30]

and metalloporphyrins, which possess a prescribable spectral feature with a strong molar ellipticity, when they are incorporated in the chiral structures or organizations, can become a spectroscopic probe for certain chiral molecular events with high sensitivity.[59] The highly symmetric square geometry of the porphyrin allows not only the construction of well-defined supramolecular architectures, but also qualitative and quantitative evaluations of the molecular orientations spectroscopically in the architectures. These characteristic features allowed us to find interesting chiroptical features of the designed porphyrin assemblies, capable of suggesting a novel concept of the chiral chemistry.

Sensing of asymmetric hydrocarbons is a challenging subject in supramolecular chemistry, since hydrocarbons do not possess functional groups appropriate for the formation of non-covalent bonds, essential for stereochemical recognition.[60] In the cases of $n = 4$ box-shaped architecture $[PyP]_2(\equiv)_4$, the requisite for extension of the π-electronic conjugation, compared with $n = 1$ and 2, is considerably small, so that the perpendicular and planar conformers form in a 1:1 ratio in a variety of solvents.[30] However, it shows strong chiroptical responses due to enrichment of R or S enantiomer of $\{\perp[PyP]_2(\equiv)_4\}_4$ in asymmetric hydrocarbons such as limonene (Figure 10a). The cyclic tetramers of $[PyP]_2(\equiv)_4$ are rather robust against dissociation, and the enantiomers of $\{\perp[PyP]_2(\equiv)_4\}_4$ were also successfully separated from one another by means of chiral HPLC on a SUMICHIRAL OA-3100 column using CH_2Cl_2/hexane (3:7) as an eluent (Figure 11).[26,61] By reference to the CD intensity at 458 nm of $\{\perp[PyP]_2(\equiv)_4\}_4$, separated as the first fraction, the enantiomeric

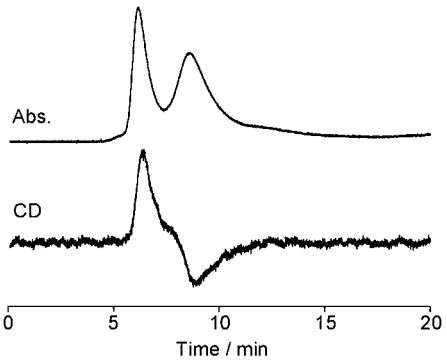

Figure 11. Chiral HPLC profiles of $\{[PyP]_2(\equiv)_4\}_4$ using CH_2Cl_2/hexane (3:7) as an eluent at 20 °C, monitored by absorption and CD responses at 455 nm.

excess of $\{\perp[PyP]_2(\equiv)_4\}_4$ in limonene (=4-isopropenyl-1-methylcyclohexane) was estimated to be at most 3%. Therefore, the successful chiroptical sensing of limonene takes great advantage of the inherently large molecular ellipticity of enantiomerically pure $\{\perp[PyP]_2(\equiv)_4\}_4$. Further, since $\{\perp[PyP]_2(\equiv)_4\}_4$ possesses also a large thermodynamic stability, a chiroptical memory, once given to $\{\perp[PyP]_2(\equiv)_4\}_4$ with (*S*)-limonene, is long-lived, even when the sample solution is diluted with (*R*)-limonene (Figure 10b). A CPK model study predicted that $\{\perp[PyP]_2(\equiv)_4\}_4$ is likely to adopt a rectangular shape, whose inner space ($1 \times 1 \times 2\,nm^3$) can accommodate 4–6 molecules of limonene. Nevertheless, for a better minimization of the vacancy of the solvent-including inner space, $\{\perp[PyP]_2(\equiv)_4\}_4$ is likely distorted in an orthorhombic manner, so that it displays an extraordinary large molecular ellipticity. The occurrence of enantiomeric enrichment of $\{\perp[PyP]_2(\equiv)_4\}_4$ allows determination of the optical purity as well as the absolute configuration of the asymmetric hydrocarbons.

4.4 Chiroptical Visualization of Vortex Flows Using a Zinc Porphyrin Supramolecular Nanofiber. Quite recently, we have found that a supramolecular polymer of J-aggregated zinc porphyrin dendrimer DP (Scheme 7) can chiroptically visualize the macroscopic chirality of a vortex, generated by mechanical rotary stirring of a fluid in an optical cell.[34,62–64] The vortex, schematically represented in Figure 12, is recognized as a macroscopic chirality and a possible origin of chiral symmetry breaking in nature. Compared with, e.g., rheometric shear flows, vortexes are complex, involving many locally different fluidic flows. For example, upon mechanical rotary stirring of a fluid in a cuvette, a tight, torsional flow is generated at the rotary center, while the peripheral part of the vortex involves a loose, spiral flow (Figure 12, left). We initially thought that the observed chiroptical activity of the sample solution must be due to the helical twisting of the individual nanofibers of J-aggregated DP in the vortex flow.[63a,63b] However, we later noticed, through a discussion with Meijer and Meskers, that this is possibly due to the consequence of a macroscopic chiral alignment of the nanofibers (Figure 12, right) upon rotary stirring.[65] A fibrous supramolecular assembly of oligo(*p*-phenylenevinylene) derivative (Scheme 7, A-OPV3), prepared by them, also showed analogous chiroptical responses in the vortex flows.[33]

DP forms a J-aggregate in benzene by a π-stacking

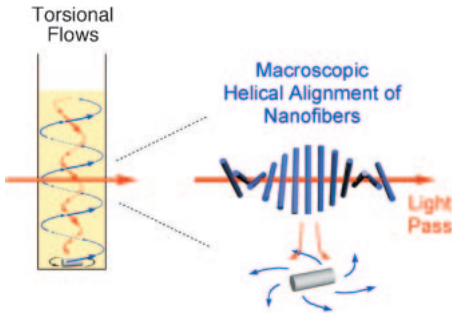

Figure 12. Schematic illustrations of torsional flows generated upon lower-side counterclockwise (CCW) rotary stirring and accompanying macroscopic helical alignment of nanofibers involved.

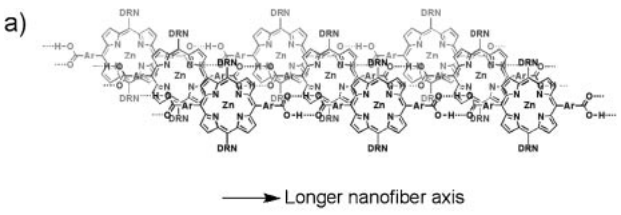

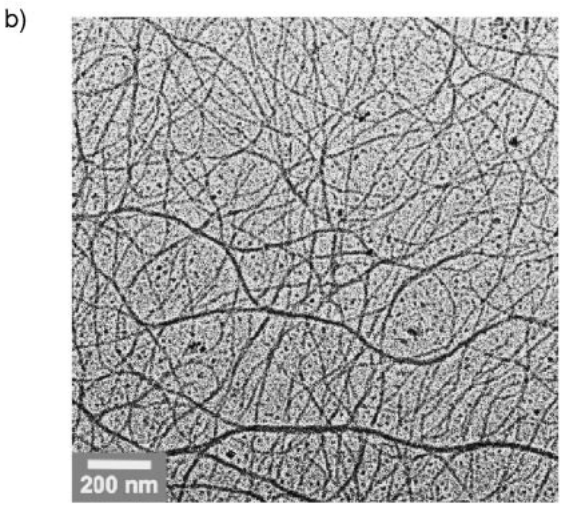

Figure 13. a) A J-aggregated form of hydrogen-bonded supramolecular polymer (nanofiber) of DP. DRN represents a dendritic wedge. b) Transmission electron micrographs (TEM) of an air-dried sample of a benzene solution of DP (1.0×10^{-5} M), deposited on a specimen grid covered with a thin carbon support film.

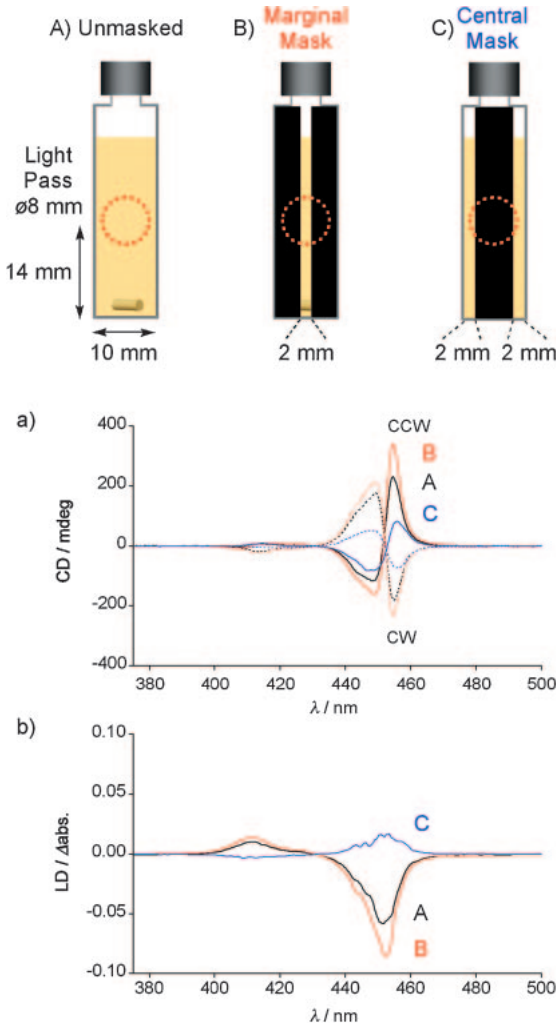

Figure 14. a) Circular dichroism (CD) and b) linear dichroism (LD) spectroscopy of a benzene solution (3.0 mL) of the nanofibers of DP (6.0×10^{-6} M), upon lower-side rotary stirring at 1350 rpm in clockwise (broken curves) or counterclockwise (solid curves) direction using a $\phi 2.0 \times 5.0$ mm Teflon-coated magnetic stirring bar at 20 °C in $10 \times 10 \times 40$ mm^3 quartz optical cells. CD and LD spectra with cells A) unmasked (black curves), B) masked at marginal parts with 4-mm wide black tapes to leave a 2-mm wide central slit (red curves), and C) masked at a vertical center with a 6-mm wide black tape (blue curves).

interaction, promoted by the formation of hydrogen bonds at its carboxylic acid side groups to give a supramolecular polymer (Figure 13a).[32] Transmission electron microscopy (TEM) of the benzene solution of DP showed 10–20 nm wide, discrete nanofibers with a very high aspect ratio (Figure 13b). While a benzene solution of DP (6.0×10^{-6} M; M = mol dm^{-3}) without stirring was CD silent, it became optically active upon mechanical rotary stirring (Figure 14a, black curves). For example, when stirred at 1350 rpm in a clockwise direction (CW), the sample solution displayed intense CD bands at the Soret absorption region due to J-aggregated DP (413, 449, and 455 nm). While very weak CD bands were observed at the Q-band region (530–610 nm), no chiroptical activity emerged at the absorption band of non-assembled DP. In order to assess this intriguing macroscopic CD effect, DP was dip-coated from its benzene solution on a thick glass plate. The dip-coated thin film showed a linear dichroism (LD) activity, where the nanofibers are oriented preferentially along the dipping direction. This nanofiber-coated glass plate was then lapped over another prepared in a manner similar to the above, and observed to CD spectroscopy. Quite interestingly, when the films were lapped in such a way that their oriented directions were angled by 45° (φ), a distinct chiroptical response appeared, whose spectral shape is virtually identical to

that observed for the stirred solution of J-aggregated DP. When the dihedral angle for lapping (φ) was changed from 45° to −45°, a spectral inversion took place. Here, we could conclude a possible major origin of the induced CD as macroscopic chiral alignment of nanofibers upon rotary stirring.[65] We then employed LD spectroscopy in order to investigate orientation of the nanofibers in the vortex flows (Figure 14b). While the sample solution ($[DP] = 6.0 \times 10^{-6}$ M), though containing long nanofibers, was LD silent without stirring, it turned LD active upon rotary stirring. Since the spectral sign is the same as that of the dip-coated film sample, placed in such a way that its oriented direction is parallel to the vertical axis of the linearly polarized incident light, it is likely that the nanofibers preferentially align perpendicularly to the rotary direction. Nevertheless, considering that the fluidic situation in a vortex, generated by rotary stirring, may change locally, we carried out point-wise LD and CD spectroscopy with optical cells selectively masked at the margins or vertical center (Figure 14, red and blue curves). Quite interestingly, while the LD sign observed through the central slit of the masked cell (Figure 14b, red curve) was identical to that of the entire solution (Figure 14b, black curve), the LD spectrum observed through the margins (Figure 14b, blue curve) was opposite in sign to the others. These observations suggest that the preferential alignments of the nanofibers flowing at the center and periphery of the vortex are different from each another. While the chiroptical response observed through the center slit (Figure 14a, red curves) was more intense than that with an unmasked cell (Figure 14a, black curves), the chiroptical response with a cell masked at its margins was much less intense (Figure 14a, blue curves). Considering the hydrodynamic model of a vortex of fluids generated in a cuvette (Figure 12, left), they perfectly render spectroscopically local different fluidic flows in a vortex. The phenomenon observed with the nanofibers of J-aggregated DP is known for cholesteric liquid crystalline materials involving a macroscopic helical alignment of mesogenic molecules.[66] However, noteworthy is that in our system, such a macroscopic helical alignment occurs in non-constraint fluid media without any assistance from rheometric flows.

5. Inorganic–Organic Nanocomposites

5.1 Inclusion Complexation of MC with Metalloporphyrins. Molybdenum blue (MB), formed by partial reduction of Mo^{VI} in an acidic aqueous solution, has been an enigmatic inorganic material due to its vivid blue color. It is a mixture of polyoxomolybdate (POM) clusters consisting of mixed-valent Mo^{V} and Mo^{VI} nuclei.[67] Although the initial exploration was made more than 200 years ago,[68] the first success in structural analysis of POM clusters was reported only recently in 1995, where Müller and co-workers isolated a wheel-shaped giant POM cluster and obtained its crystal structure.[35b] To date, they have also succeeded in structural determination of large POM clusters with hollow and spherical shapes.[69] Despite their interesting potential in material science, no examples had been reported for utilization of such inorganic nano-objects for the fabrication of discrete inorganic/organic nanocomposite materials. With this background, we have demonstrated the first example of a discrete inorganic/organic nanocomposite from nanoscale POM.[36] The wheel-shaped polyoxomolybdate clusters MC,[35a] upon mixing with metalloporphyrins with *meso*-aminophenyl substituents, were found to form discrete inclusion complexes, where the inorganic cavity of MC can accommodate up to three molecules of the guest compounds, to give spatially isolated metalloporphyrin deckers (Scheme 8). MC with the chemical formula $Na_{(32-n)}[(MoO_3)_{176}(H_2O)_{63}(MeOH)_{17}H_n]\cdot$ca. $600H_2O\cdot$ca. 30MeOH possesses a large cavity with a diameter of approximately 2.3 nm.[35a] We have expected that this cavity can include 1) proton-acceptors via a hydrogen-bonding interaction and 2) cationic species via electrostatic interactions, since a great number of proton-donating O–H species are concentrated at the surface.

MC is highly soluble in MeCN to give a blue-colored clear solution, which shows characteristic broad absorption bands at 730 and 1058 nm. The absorption spectroscopy indicated that a zinc complex of 5,10,15,20-tetrakis(4-aminophenyl)porphyrin (TAP) interacts with MC in MeCN. For example, upon titration of TAP with MC, the Soret-band of TAP at 430 nm decreases in intensity with a small blue shift toward 427 nm, while a red-shifted shoulder appears at 440 nm. The characteristic absorption bands of MC at 730 and 1058 nm also decreased in intensity with a red shift. To determine the stoichiometry of the complexation, spectroscopic titration of MC with TAP was conducted in MeCN, where MC showed stepwise spectral changes in response to [TAP]/[MC] at 0–2, 2–4, and 4–10, with isosbestic points at 1121, 1138, and 1143 nm, respectively (Figure 15). This observation indicates the stepwise formation of 1:1, 1:2, and 1:3 complexes between MC and TAP. These absorption spectral studies thus strongly indicate that MC accommodates TAP inside the cavity via the formation of multiple hydrogen bonds, to give inclusion complexes $MC\supset TAP_{1-3}$.

Ultrahigh-vacuum scanning tunneling microscopy (UHV-STM) (Figure 16) demonstrated that the product upon complexation of MC with TAP is indeed an inclusion complex $MC\supset TAP$.[70] Thus, a dilute aqueous solution of a mixture of MC and TAP (1:3) was sprayed by pulse injection onto a clear flat (111) surface of Cu. The UHV-STM image at 80 K showed the presence of numerous doughnut-like discrete nano-objects with a diameter of 4–5 nm, which is consistent with the reported dimension of crystallographically-defined MC.[35a] Interestingly, some of these nano-objects in the STM image appear to possess a filled cavity. By means of scanning tunneling spectroscopy (STS) on one of these filled objects,[71] correlations between differential conductance (dI/dV) and sample bias voltage (V_s) were measured separately for the shell and core. These two parts exhibit essentially different $dI/dV - V_s$ profiles from one another. Although the shell, similarly to intact MC, displays a gradual increase in dI/dV with either decreasing or increasing V_s, the core in contrast, shows two bands at −0.7 and +1.6 V, which are assignable to resonant tunneling currents via the HOMO and LUMO of the guest compound.[72] Since the energy gap of 2.3 eV thus observed is consistent with an optical HOMO–LUMO energy gap of TAP (2.1 eV), it is obvious that the object with a filled cavity is $MC\supset TAP$.

5.2 Inorganic/Organic Polypseudorotaxane. With the background in successful construction of the inorganic/organic inclusion complex, we have further designed an oligomeric *p*-

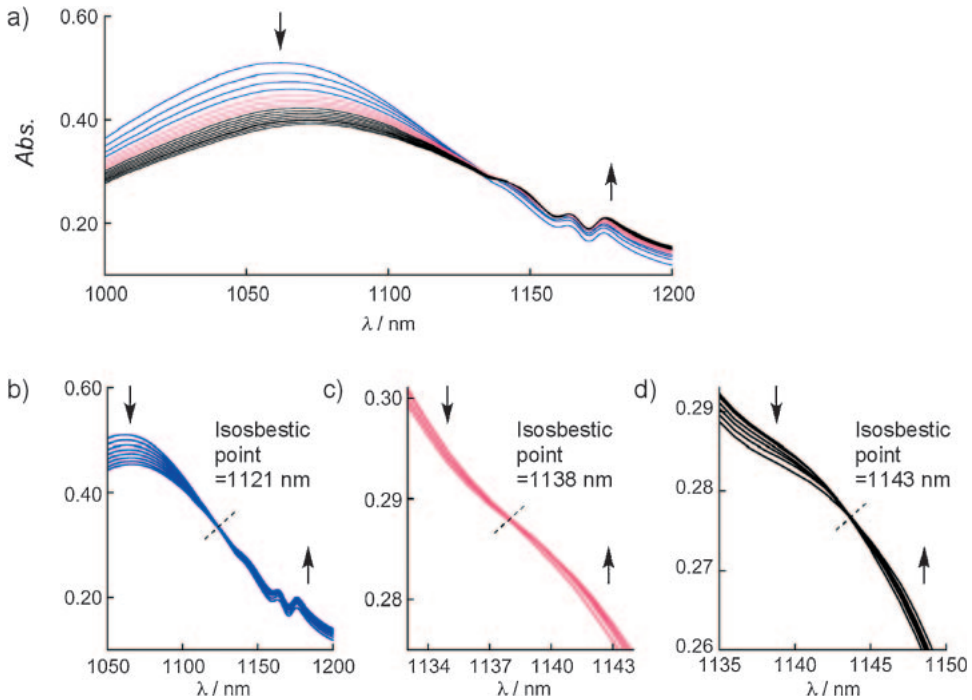

Figure 15. Spectroscopic titration of MC (2.5×10^{-6} M) with TAP in MeCN at 20 °C. [TAP] = a) 0–2.1×10^{-5} M (overall spectral change), b) 0–0.5×10^{-5} M, c) 0.6×10^{-5}–1.0×10^{-5} M, and d) 1.2×10^{-5}–2.1×10^{-5} M.

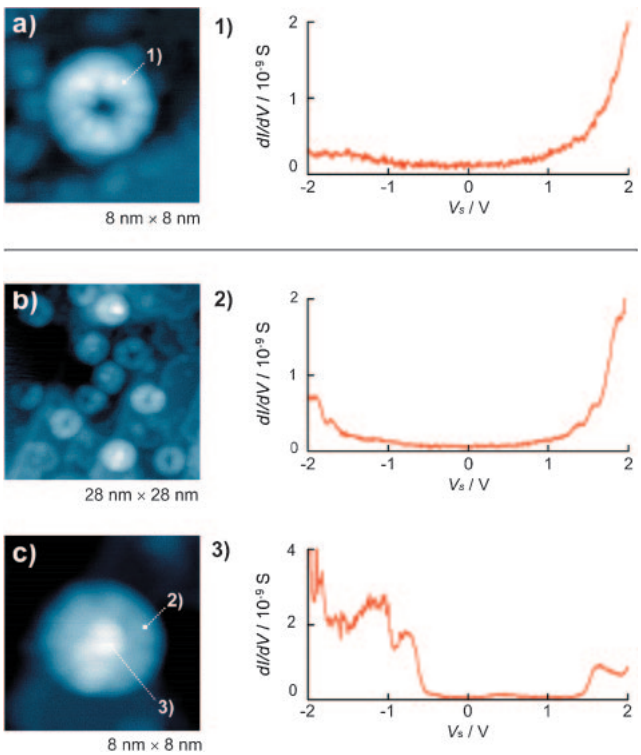

Figure 16. Ultrahigh-vacuum scanning tunneling microscopy (UHV-STM) and scanning tunneling spectroscopy (STS) on Cu(111) surfaces at 80 K. UHV-STM of a) intact MC (imaging conditions: $I = 2.0$ pA, $V_s = 1.0$ V), b) a 1:3 mixture of MC and TAP ($I = 2.0$ pA, $V_s = 3.0$ V), and c) MC⊃TAP ($I = 2.0$ pA, $V_s = 1.0$ V). Differential conductance (dI/dV)–sample bias voltage (V_s) correlations in STS of 1) intact MC observed in a), 2) and 3) MC⊃TAP observed in c).

phenylenebutadiynylene rigid rod molecule bearing ammonium ion pendants (PB_n) with an expectation that it may one-dimensionally connect multiple MC rings in a cofacial manner by an electrostatic interaction (Scheme 9). Successful fabrication of a novel one-dimensional (1D) nano-object, having a polypseudorotaxane structure was observed upon threading multiple MC rings by a PB_n rod.[37] Although a variety of organic polypseudorotaxanes have been reported,[73–77] inorganic/organic hybrid polyrotaxanes are unprecedented.

For the synthesis of PB_n, a 1,4-diethynylbenzene derivative with four *tert*-butoxycarbonyl-protected amino groups ($^{BOC}PB_1$) was subjected to Cu^{II}-mediated Glaser-Hey coupling,[78] and a high molecular-weight fraction of the resultant polymer ($^{BOC}PB_n$) was isolated by preparative size-exclusion chromatography (SEC) and deprotected with TFA. By using the analytical SEC profile of an oligomeric fraction of the coupling product as the calibration standard, the average number of the repeating PB units (n) of isolated $^{BOC}PB_n$ and its polydispersity were estimated as 14 (average length = 14 nm) and 1.5, respectively.

For the coassembly of MC with PB_{14}, a MeOH solution of PB_{14} ([PB unit] = 6.0×10^{-5} M) was mixed with an MeCN solution of MC (0.5×10^{-5} M) at [PB unit]/[MC] = 3 (MeCN/MeOH = 4/1 v/v), and the resulting mixture was stirred for 10 min at 20 °C. Dynamic light scattering (DLS) analysis indicated that the mixture contains large objects with a size regime ranging from 50 to 3500 nm (average radius; 347 nm). Transmission electron microscopy (TEM) of an air-dried sample of the solution clearly displayed the presence of one-dimensional (1D) objects with a high aspect ratio (Figure 17). While most 1D objects visualized by TEM are much longer than PB_{14} with an average length of 14 nm (vide infra), they are characterized by a uniform diameter of 4 nm,

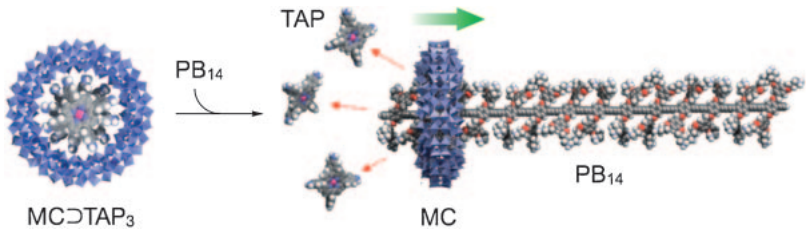

Scheme 10. Schematic illustration of the possible liberation of TAP from $MC \supset TAP_3$ upon threading of PB_{14}.

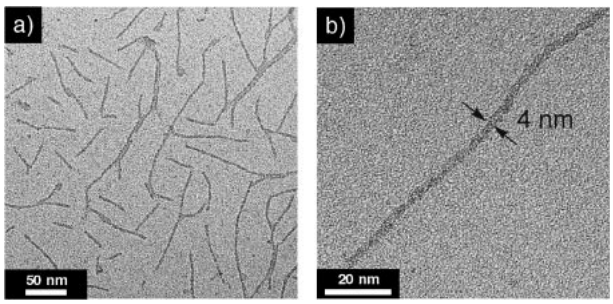

Figure 17. TEM micrographs of air-dried MeCN/MeOH (4/1 v/v) solutions of a mixture of MC and PB_{14} ([PB unit]/[MC] = 3), deposited on a specimen grid covered with a thin carbon support film. [PB unit] = 1.2×10^{-5} M, [MC] = 0.4×10^{-5} M.

which is nearly identical to that of MC.[35a]

In an absorption spectral study, when MC was added to an MeCN/MeOH (4/1 v/v) solution of PB_{14} ([PB unit]/[MC] = 3), a visible absorption band of PB_{14} became less intensified and broaden. While PB_{14} upon excitation at 440 nm emitted a blue-colored fluorescence centered at 480 nm, addition of MC efficiently quenched the photoexcited state of PB_{14}. In order to address the role of ring-shaped structure of MC, we attempted coassembly of guest-included $MC \supset TAP_{1-3}$ ([TAP]/[MC] = 3) with PB_{14} in the fluorescence spectroscopy. $MC \supset TAP_{1-3}$ also hardly showed red fluorescence at 600–750 nm originating from TAP (Figure 18, black solid curve), as a consequence of the photochemical quenching of the singlet excited state of included TAP by MC. However, when $MC \supset TAP_{1-3}$ was mixed with PB_{14} in MeCN/MeOH (4/1 v/v), TAP recovered its red fluorescence (Figure 18), indicating that TAP binds MC less strongly than PB_{14} and is kicked out from the MC cavity upon mixing $MC \supset TAP_{1-3}$ with PB_{14} (Scheme 10). This result indicates that the threading of the MC rings with PB_{14} is quite essential for their controlled 1D coassembly. Here, we also assume that the threaded MC units are stitched together by the surface adhesion of PB_{14}, and such short-chain 1D objects are occasionally connected to one another. Consequently, they become much longer than expected from the average length (14 nm) of PB_{14} as template. Since MC is a mixed-valent inorganic cluster with chromophoric character, exploration of optoelectronic properties of this novel 1D nanocomposite material is a subject worthy of further investigation.[79]

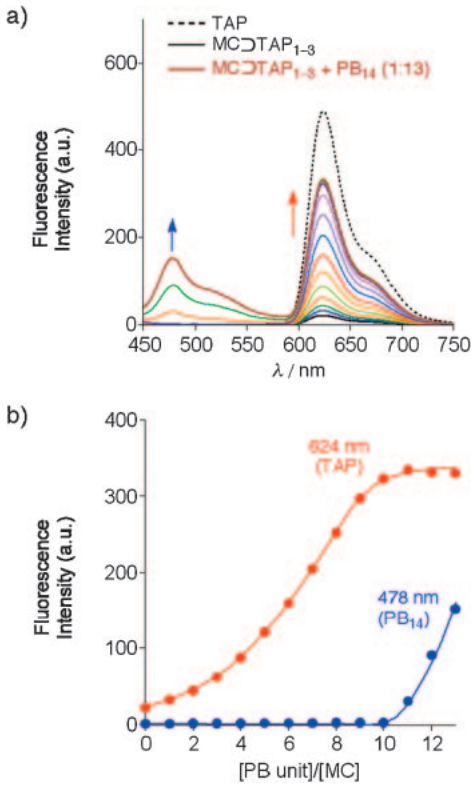

Figure 18. a) Fluorescence spectra of PB_{14} (λ_{ext}; 435 nm) in MeCN/MeOH (4/1 v/v) at 20 °C upon titration of $MC \supset TAP_{1-3}$ (a 1:3 mixture of MC and TAP) with PB_{14}. b) Plots of the fluorescence intensities of PB_{14} at 478 nm (blue filled circles) and TAP at 624 nm (red filled circles) versus [PB unit]/[MC]. [MC] = 6.1×10^{-7} M.

6. Conclusion

We have designed a variety of metalloporphyrin nanoclusters, connected via covalent or noncovalent linkages, with an objective to find/develop their potential properties and functions. π-Electrons as well as metal centers of the metalloporphyrin derivatives determine the basic electronic properties, related to optical, magnetic, and conductive properties, and assembling events. Their unique self-assembling behaviors, which can dynamically transform its structure, allow sensing of chemical and physical stimuli such as molecular recognition, solvent polarity, light, temperature, magnetic force fields, and hydrodynamic interactions. By understanding the basic electronic structure and the self-assembling events of artificial metalloporphyrin nanoarchitectures, we have achieved their functionalization, but in most cases serendipitously found unexpected specific functions in the course of study. Our achievements, described in this review article, suggest the importance of the "molecular design" from the viewpoints of both covalent and noncovalent chemistry.

The author expresses his sincerest appreciation to Prof. Takuzo Aida (The University of Tokyo) and Prof. Atsuhiro Osuka (Kyoto University) for their continuous support and guidance. The author thanks his collaborators listed in the references, in particular Dr. Md. Akhtarul Alam, for his considerable experimental contribution in this work.

References

1 a) A. Huijser, B. M. J. M. Suijkerbuijk, R. J. M. K. Gebbink, T. J. Savenije, L. D. A. Siebbeles, *J. Am. Chem. Soc.* **2008**, *130*, 2485. b) J.-F. Gnichwitz, M. Wielopolski, K. Hartnagel, U. Hartnagel, D. M. Guldi, A. Hirsch, *J. Am. Chem. Soc.* **2008**, *130*, 8491. c) C. M. Drain, *Proc. Natl. Acad. Sci. U.S.A.* **2002**, *99*, 5178.

2 a) C. Röger, M. G. Müller, M. Lysetska, Y. Miloslavina, A. R. Holzwarth, F. Würthner, *J. Am. Chem. Soc.* **2006**, *128*, 6542. b) F. Würthner, *Chem. Commun.* **2004**, 1564–1579, and references therein.

3 a) J. P. Hill, W. Jin, A. Kosaka, T. Fukushima, H. Ichihara, T. Shimomura, K. Ito, T. Hashizume, N. Ishii, T. Aida, *Science* **2004**, *304*, 1481. b) Y. Yamamoto, T. Fukushima, Y. Suna, N. Ishii, A. Saeki, S. Seki, S. Tagawa, M. Taniguchi, T. Kawai, T. Aida, *Science* **2006**, *314*, 1761.

4 M. Takase, V. Enkelmann, D. Sebastiani, M. Baumgarten, K. Müllen, *Angew. Chem., Int. Ed.* **2007**, *46*, 5524.

5 M. Williams-Harry, A. Bhaskar, G. Ramakrishna, T. Goodson, III, M. Imamura, A. Mawatari, K. Nakao, H. Enozawa, T. Nishinaga, M. Iyoda, *J. Am. Chem. Soc.* **2008**, *130*, 3252.

6 Z. S. Yoon, J. H. Kwon, M.-C. Yoon, M. K. Koh, S. B. Noh, J. L. Sessler, J. T. Lee, D. Seidel, A. Aguilar, S. Shimizu, M. Suzuki, A. Osuka, D. Kim, *J. Am. Chem. Soc.* **2006**, *128*, 14128.

7 a) M. Stępien, B. Donnio, J. L. Sessler, *Angew. Chem., Int. Ed.* **2007**, *46*, 1431. b) P. J. Boul, D.-G. Cho, G. M. A. Rahman, M. Marquez, Z. Ou, K. M. Kadish, D. M. Guldi, J. L. Sessler, *J. Am. Chem. Soc.* **2007**, *129*, 5683.

8 a) A. W. Roszak, T. D. Howard, J. Southall, A. T. Gardiner, C. J. Law, N. W. Isaacs, R. J. Cogdell, *Science* **2003**, *302*, 1969. b) J. Koepke, X. Hu, C. Muenke, K. Schulten, H. Michel, *Structure* **1996**, *4*, 581. c) G. McDermott, S. M. Prince, A. A. Freer, A. M. Hawthornthwaite-Lowless, M. Z. Papiz, R. J. Cogdell, N. W. Isaacs, *Nature* **1995**, *374*, 517.

9 M. F. Perutz, *Nature* **1970**, *228*, 726.

10 J. P. Collman, R. R. Gagne, C. A. Reed, T. R. Halbert, G. Lang, W. T. Robinson, *J. Am. Chem. Soc.* **1975**, *97*, 1427.

11 J. Wojaczynski, L. Latos-Grazynski, *Coord. Chem. Rev.* **2000**, *204*, 113.

12 Y. Nakamura, N. Aratani, A. Osuka, *Chem. Soc. Rev.* **2007**, *36*, 831.

13 Y. Kobuke, K. Ogawa, *Bull. Chem. Soc. Jpn.* **2003**, *76*, 689.

14 A. Tsuda, A. Nakano, H. Furuta, H. Yamochi, A. Osuka, *Angew. Chem., Int. Ed.* **2000**, *39*, 558.

15 A. Tsuda, H. Furuta, A. Osuka, *Angew. Chem., Int. Ed.* **2000**, *39*, 2549.

16 A. Tsuda, H. Furuta, A. Osuka, *J. Am. Chem. Soc.* **2001**, *123*, 10304.

17 A. Tsuda, A. Osuka, *Science* **2001**, *293*, 79.

18 A. Tsuda, A. Osuka, *Adv. Mater.* **2002**, *14*, 75.

19 a) M.-C. Yoon, S. B. Noh, A. Tsuda, Y. Nakamura, A. Osuka, D. Kim, *J. Am. Chem. Soc.* **2007**, *129*, 10080. b) A. Tsuda, Y. Nakamura, A. Osuka, *Chem. Commun.* **2003**, 1096.

20 A. Osuka, H. Shimidzu, *Angew. Chem., Int. Ed. Engl.* **1997**, *36*, 135.

21 T. Ogawa, Y. Nishimoto, N. Yoshida, N. Ono, A. Osuka, *Angew. Chem., Int. Ed.* **1999**, *38*, 176.

22 a) A. Tsuda, T. Oshima, *J. Org. Chem.* **2002**, *67*, 1282. b) A. Tsuda, T. Oshima, *New J. Chem.* **1998**, *22*, 1027.

23 A. Tsuda, C. Fukumoto, T. Oshima, *J. Am. Chem. Soc.* **2003**, *125*, 5811.

24 a) H. Sato, K. Tashiro, H. Shinmori, A. Osuka, T. Aida, *Chem. Commun.* **2005**, 2324. b) H. Sato, K. Tashiro, H. Shinmori, A. Osuka, Y. Murata, K. Komatsu, T. Aida, *J. Am. Chem. Soc.* **2005**, *127*, 13086.

25 a) F. Cheng, S. Zhang, A. Adronov, L. Echegoyen, F. Diederich, *Chem.—Eur. J.* **2006**, *12*, 6062. b) D. Bonifazi, M. Scholl, F. Song, L. Echegoyen, G. Accorsi, N. Armaroli, F. Diederich, *Angew. Chem., Int. Ed.* **2003**, *42*, 4966.

26 a) I.-W. Hwang, T. Kamada, T. K. Ahn, D. M. Ko, T. Nakamura, A. Tsuda, A. Osuka, D. Kim, *J. Am. Chem. Soc.* **2004**, *126*, 16187. b) A. Tsuda, T. Nakamura, S. Sakamoto, K. Yamaguchi, A. Osuka, *Angew. Chem., Int. Ed.* **2002**, *41*, 2817.

27 A. Tsuda, H. Hu, R. Watanabe, T. Aida, *J. Porphyrins Phthalocyanines* **2003**, *7*, 388.

28 A. Tsuda, H. Hu, R. Tanaka, T. Aida, *Angew. Chem., Int. Ed.* **2005**, *44*, 4884.

29 J. Aimi, Y. Nagamine, A. Tsuda, A. Muranaka, M. Uchiyama, T. Aida, *Angew. Chem., Int. Ed.* **2008**, *47*, 5153.

30 J. Aimi, K. Oya, A. Tsuda, T. Aida, *Angew. Chem., Int. Ed.* **2007**, *46*, 2031.

31 A. Tsuda, S. Sakamoto, K. Yamaguchi, T. Aida, *J. Am. Chem. Soc.* **2003**, *125*, 15722.

32 T. Yamaguchi, T. Kimura, H. Matsuda, T. Aida, *Angew. Chem., Int. Ed.* **2004**, *43*, 6350.

33 M. Wolffs, S. J. George, Z. Tomović, S. C. J. Meskers, A. P. H. J. Schenning, E. W. Meijer, *Angew. Chem., Int. Ed.* **2007**, *46*, 8203.

34 A. Tsuda, M. A. Alam, T. Harada, T. Yamaguchi, N. Ishii, T. Aida, *Angew. Chem., Int. Ed.* **2007**, *46*, 8198.

35 a) A. Müller, M. Koop, H. Bögge, M. Schmidtmann, C. Beugholt, *Chem. Commun.* **1998**, 1501. b) A. Müller, E. Krickermeyer, J. Meyer, H. Bögge, F. Peters, W. Plass, E. Diemann, S. Dillinger, F. Nonnenbruch, M. Randerath, C. Menke, *Angew. Chem., Int. Ed. Engl.* **1995**, *34*, 2122.

36 A. Tsuda, E. Hirahara, Y.-S. Kim, H. Tanaka, T. Kawai, T. Aida, *Angew. Chem., Int. Ed.* **2004**, *43*, 6327.

37 M. A. Alam, Y.-S. Kim, S. Ogawa, A. Tsuda, N. Ishii, T. Aida, *Angew. Chem., Int. Ed.* **2008**, *47*, 2070.

38 a) M. G. H. Vicente, L. Jaquinod, K. M. Smith, *Chem. Commun.* **1999**, 1771. b) M. J. Crossley, L. J. Govenlock, J. K. Prashar, *J. Chem. Soc., Chem. Commun.* **1995**, 2379. c) N. Kobayashi, M. Numao, R. Kondo, S. Nakajima, T. Osa, *Inorg. Chem.* **1991**, *30*, 2241.

39 a) G. Sedghi, K. Sawada, L. J. Esdaile, M. Hoffmann, H. L. Anderson, D. Bethell, W. Haiss, S. J. Higgins, R. J. Nichols, *J. Am. Chem. Soc.* **2008**, *130*, 8582. b) M. Drobizhev, Y. Stepanenko, A. Rebane, C. J. Wilson, T. E. O. Screen, H. L. Anderson, *J. Am. Chem. Soc.* **2006**, *128*, 12432.

40 D. P. Arnold, D. A. James, *J. Org. Chem.* **1997**, *62*, 3460.

41 V. S. Lin, S. G. DiMagno, M. J. Therien, *Science* **1994**, *264*, 1105.

42 L. J. Esdaile, P. Jensen, J. C. McMurtrie, D. P. Arnold, *Angew. Chem., Int. Ed.* **2007**, *46*, 2090.

43 a) N. Aratani, A. Osuka, Y. H. Kim, D. H. Jeong, D. Kim,

Angew. Chem., Int. Ed. **2000**, *39*, 1458. b) N. Yoshida, N. Aratani, A. Osuka, *Chem. Commun.* **2000**, 197.

44 M. Gouterman, *The Porphyrins*, Academic Press, New York, **1978**, Vol. III.

45 K. Sugiura, T. Matsumoto, S. Ohkouchi, Y. Naitoh, T. Kawai, Y. Takai, K. Ushiroda, Y. Sakata, *Chem. Commun.* **1999**, 1957.

46 a) R. H. Martin, M.-J. Marchant, *Tetrahedron* **1974**, *30*, 347. b) C. Goediche, H. Stegemeyer, *Tetrahedron Lett.* **1970**, *11*, 937.

47 N. Yoshida, T. Ishizuka, A. Osuka, D. H. Jeong, H. S. Cho, D. Kim, Y. Matsuzaki, A. Nogami, K. Tanaka, *Chem.—Eur. J.* **2003**, *9*, 58.

48 M. Kamo, A. Tsuda, Y. Nakamura, N. Aratani, K. Furukawa, T. Kato, A. Osuka, *Org. Lett.* **2003**, *5*, 2079.

49 R. E. Martin, F. Diederich, *Angew. Chem., Int. Ed.* **1999**, *38*, 1350.

50 A. Osuka, K. Maruyama, *J. Am. Chem. Soc.* **1988**, *110*, 4454.

51 K. Yamaguchi, *J. Mass Spectrom.* **2003**, *38*, 473.

52 A similar cyclotetramerization has been reported for [5-(2-aminopyrimidin-5-yl)-10,20-bis(3,5-di-*tert*-butylphenyl)porphyrinato]zinc. T. S. Balaban, R. Goddard, M. Linke-Schaetzel, J.-M. Lehn, *J. Am. Chem. Soc.* **2003**, *125*, 4233.

53 a) X. Chi, A. J. Guerin, R. A. Haycock, C. A. Hunter, L. D. Sarson, *J. Chem. Soc., Chem. Commun.* **1995**, 2567. b) K. Funatsu, A. Kimura, T. Imamura, Y. Sasaki, *Chem. Lett.* **1995**, 765.

54 a) K. Suzuki, M. Kawano, M. Fujita, *Angew. Chem., Int. Ed.* **2007**, *46*, 2819. b) Y. Tokunaga, D. M. Rudkevich, J. Stantamaría, G. Hilmersson, J. Rebek, Jr., *Chem.—Eur. J.* **1998**, *4*, 1449.

55 C. Reichardt, *Chem. Rev.* **1994**, *94*, 2319.

56 D. G. Yablon, A. M. Schilowitz, *Appl. Spectrosc.* **2004**, *58*, 843.

57 a) E. Yashima, K. Maeda, T. Nishimura, *Chem.—Eur. J.* **2004**, *10*, 42, and references therein. b) D. J. Cram, J. M. Cram, *Acc. Chem. Res.* **1978**, *11*, 8, and references therein.

58 a) E. Yashima, K. Maeda, Y. Okamoto, *Nature* **1999**, *399*, 449. b) J. C. Nelson, J. G. Saven, J. S. Moore, P. G. Wolynes, *Science* **1997**, *277*, 1793.

59 a) V. V. Borovkov, J. M. Lintuluoto, M. Fujiki, Y. Inoue, *J. Am. Chem. Soc.* **2000**, *122*, 4403. b) X. Huang, B. H. Rickman, B. Borhan, N. Berova, K. Nakanishi, *J. Am. Chem. Soc.* **1998**, *120*, 6185. c) M. Takeuchi, T. Imada, S. Shinkai, *Angew. Chem., Int. Ed.* **1998**, *37*, 2096. d) Y. Furusho, T. Kimura, Y. Mizuno, T. Aida, *J. Am. Chem. Soc.* **1997**, *119*, 5267.

60 a) T. Kawasaki, H. Tanaka, T. Tsutsumi, T. Kasahara, I. Sato, K. Soai, *J. Am. Chem. Soc.* **2006**, *128*, 6032. b) R. Paolesse, D. Monti, L. La Monica, M. Venanzi, A. Froiio, S. Nardis, C. Di Natale, E. Martinelli, A. D'Amico, *Chem.—Eur. J.* **2002**, *8*, 2476. c) R. B. Prince, S. A. Barnes, J. S. Moore, *J. Am. Chem. Soc.* **2000**, *122*, 2758. d) K. Kobayashi, Y. Asakawa, Y. Kikuchi, H. Toi, Y. Aoyama, *J. Am. Chem. Soc.* **1993**, *115*, 2648.

61 T. Kamada, N. Aratani, T. Ikeda, N. Shibata, Y. Higuchi, A. Wakamiya, S. Yamaguchi, K. S. Kim, Z. S. Yoon, D. Kim, A. Osuka, *J. Am. Chem. Soc.* **2006**, *128*, 7670.

62 a) Related references for crystallizations: D. K. Kondepudi, J. Laudadio, K. Asakura, *J. Am. Chem. Soc.* **1999**, *121*, 1448. b) D. K. Kondepudi, R. J. Kaufman, N. Singh, *Science* **1990**, *250*, 975.

63 a) Related references for porphyrin J-aggregates: C. Escudero, J. Crusats, I. Díez-Pérez, Z. El-Hachemi, J. M. Ribó, *Angew. Chem., Int. Ed.* **2006**, *45*, 8032. b) J. M. Ribó, J. Crusats, F. Sagués, J. Claret, R. Rubires, *Science* **2001**, *292*, 2063. c) O. Ohno, Y. Kaizu, H. Kobayashi, *J. Chem. Phys.* **1993**, *99*, 4128.

64 Related references for cyanine dye assemblies: U. D. Rossi, S. Dähne, S. C. J. Meskers, H. P. J. M. Dekkers, *Angew. Chem., Int. Ed. Engl.* **1996**, *35*, 760.

65 Y. Shindo, Y. Ohmi, *J. Am. Chem. Soc.* **1985**, *107*, 91.

66 a) F. D. Saeva, P. E. Sharpe, G. R. Olin, *J. Am. Chem. Soc.* **1973**, *95*, 7656. b) F. D. Saeva, J. J. Wysocki, *J. Am. Chem. Soc.* **1971**, *93*, 5928.

67 a) F. B. Schirmer, Jr., L. F. Audrieth, S. T. Gross, D. S. McClellan, L. J. Seppi, *J. Am. Chem. Soc.* **1942**, *64*, 2543. b) J. J. Berzelius, *Ann. Phys. Chem.* **1826**, *6*, 369.

68 C. W. Scheele, in *Sämtliche Physische und Chemische Werke*, ed. by D. S. F. Hermbstädt, Martin Sändig oHG: Niederwalluf/Wiesbaden, **1971**, Vol. 1, pp. 185–200.

69 a) A. Müller, S. Roy, *Coord. Chem. Rev.* **2003**, *245*, 153. b) A. Müller, C. Serain, *Acc. Chem. Res.* **2000**, *33*, 2.

70 a) H. Tanaka, T. Kawai, *Surf. Sci.* **2003**, *539*, L531. b) H. Tanaka, T. Kawai, *J. Vac. Sci. Technol., B* **1997**, *15*, 602.

71 a) P. Guaino, A. A. Cafolla, O. McDonald, D. Carty, G. Sheerin, G. Hughes, *J. Phys.: Condens. Matter* **2003**, *15*, S2693. b) M. Pomerantz, A. Aviram, R. A. McCorkle, L. Li, A. G. Schrott, *Science* **1992**, *255*, 1115.

72 L. Scudiero, D. E. Barlow, K. W. Hipps, *J. Phys. Chem. B* **2002**, *106*, 996.

73 a) A. Harada, J. Li, M. Kamachi, *Nature* **1992**, *356*, 325. b) N. Ogata, K. Sanui, J. Wada, *J. Polym. Sci., Polym. Lett. Ed.* **1976**, *14*, 459.

74 a) Reviews: M. J. Frampton, H. L. Anderson, *Angew. Chem., Int. Ed.* **2007**, *46*, 1028. b) G. Wenz, B.-H. Han, A. Müller, *Chem. Rev.* **2006**, *106*, 782.

75 a) N. Watanabe, T. Yagi, N. Kihara, T. Takata, *Chem. Commun.* **2002**, 2720. b) P. R. Ashton, P. T. Glink, M.-V. Martínez-Díaz, J. F. Stoddart, A. J. P. White, D. J. Williams, *Angew. Chem., Int. Ed. Engl.* **1996**, *35*, 1930.

76 P. E. Mason, I. W. Parsons, M. S. Tolley, *Angew. Chem., Int. Ed. Engl.* **1996**, *35*, 2238.

77 S. Choi, J. W. Lee, Y. H. Ko, K. Kim, *Macromolecules* **2002**, *35*, 3526.

78 T. Mangel, A. Eberhardt, U. Scherf, U. H. F. Bunz, K. Müllen, *Macromol. Rapid Commun.* **1995**, *16*, 571.

79 Y. Yamamoto, T. Fukushima, Y. Suna, N. Ishii, A. Saeki, S. Seki, S. Tagawa, M. Taniguchi, T. Kawai, T. Aida, *Science* **2006**, *314*, 1761.

Akihiko Tsuda was born in Osaka, Japan in 1973. He received his B.S. degree in Organic Chemistry from Shinshu University in 1997, and then received his M.S. degree in Supramolecular Chemistry from Osaka University in 1999. He obtained his Ph.D. in Organic Chemistry under the direction of Professor Atsuhiro Osuka from Kyoto University in 2002. He started his academic career as a Research Associate and an Assistant Professor with Professor Takuzo Aida at the University of Tokyo in 2002. In 2008, he was promoted to Associate Professor of the Department of Chemistry, Graduate School of Science, Kobe University. His research interests include (1) design and application of functional molecular architectures, (2) inorganic–organic nanocomposites, and (3) chiral science of supramolecular assemblies. He is also a researcher of the PRESTO (JST) program on "Structure Control and Function." He has received The Chemical Society of Japan Award for Young Chemists in 2007.